

c+ production in pp and in p -Pb collisions at sNN =5.02 TeV

Original

c+ production in pp and in p -Pb collisions at sNN =5.02 TeV / Acharya, S; Adamova, D.; Adolphson, J; Aggarwal, M.; Rinella, G.; Agnello, M.; Agrawal, N; Bufalino, S.; Concas, M.; Catalano, F.; Fecchio, P.; Balbino, A.. - In: PHYSICAL REVIEW C. - ISSN 2469-9985. - STAMPA. - 104:5(2021). [10.1103/PhysRevC.104.054905]

Availability:

This version is available at: 11583/2962435 since: 2022-05-02T21:42:08Z

Publisher:

American Physical Society

Published

DOI:10.1103/PhysRevC.104.054905

Terms of use:


This article is made available under terms and conditions as specified in the corresponding bibliographic description in the repository

Publisher copyright

(Article begins on next page)

Λ_c^+ production in pp and in p -Pb collisions at $\sqrt{s_{NN}} = 5.02$ TeV

S. Acharya *et al.**
(ALICE Collaboration)

 (Received 22 December 2020; revised 4 August 2021; accepted 23 September 2021; published 9 November 2021)

The production cross section of prompt Λ_c^+ charm baryons was measured with the ALICE detector at the LHC at midrapidity in proton-proton (pp) and proton-lead (p -Pb) collisions at a center-of-mass energy per nucleon pair of $\sqrt{s_{NN}} = 5.02$ TeV. The Λ_c^+ and $\bar{\Lambda}_c^-$ baryons were reconstructed in the hadronic decay channels $\Lambda_c^+ \rightarrow pK^-\pi^+$ and $\Lambda_c^+ \rightarrow pK_S^0$ and respective charge conjugates. The measured differential cross sections as a function of transverse momentum (p_T) and the p_T -integrated Λ_c^+ production cross section in pp and in p -Pb collisions are presented. The Λ_c^+ nuclear modification factor (R_{pPb}), calculated from the cross sections in pp and in p -Pb collisions, is presented and compared with the R_{pPb} of D mesons. The Λ_c^+/D^0 ratio is also presented and compared with the light-flavor baryon-to-meson ratios p/π and Λ/K_S^0 , and measurements from other LHC experiments. The results are compared to predictions from model calculations and Monte Carlo event generators.

DOI: [10.1103/PhysRevC.104.054905](https://doi.org/10.1103/PhysRevC.104.054905)

I. INTRODUCTION

In hadronic collisions, heavy quarks (charm and beauty) are created predominantly in hard scattering processes, and therefore the measurement of charm and beauty hadron production is a powerful test of perturbative quantum chromodynamics (pQCD) calculations. Theoretical predictions based on the QCD factorization approach describe the heavy-flavor hadron production cross section as a convolution of parton distribution functions, parton hard-scattering cross sections, and fragmentation functions. The measurements of D - and B -meson production cross sections in pp collisions at center-of-mass energies between 200 GeV and 13 TeV at RHIC [1], Tevatron [2–4], and the LHC [5–9] are generally described within uncertainties by perturbative calculations at next-to-leading order with next-to-leading-log resummation, such as the general-mass variable-flavor-number scheme (GM-VFNS [10,11]) and fixed-order next-to-leading-log (FONLL [12,13]), over a wide range of transverse momentum (p_T).

The measurement of the relative production of different heavy-flavor hadron species is also sensitive to the charm- and beauty-quark fragmentation and heavy-flavor hadron formation processes. In particular, measurements of the Λ_c^+ production cross section relative to D mesons provide insight into the hadronization of charm quarks into baryons. A measurement of Λ_c^+ baryon production at midrapidity in pp collisions at $\sqrt{s} = 7$ TeV was reported by the ALICE Collaboration in Ref. [14]. The Λ_c^+/D^0 ratio was found to be substantially higher than previous measurements at lower

energies in electron-positron (e^+e^-) [15–18] and electron-proton (e^-p) [19–21] collisions, challenging the assumption that the probabilities for a charm quark to hadronize into a specific charm hadron (fragmentation fractions) are universal among different collision systems [22]. In addition, the Λ_c^+/D^0 ratio was compared with predictions from several Monte Carlo (MC) generators, which implement different fragmentation processes, such as the formation of strings (PYTHIA [23,24]), ropes (DIPSY [25,26]), or baryonic clusters (HERWIG [27]), where the fragmentation parameters for these simulations are tuned to previous e^+e^- and e^-p collision measurements. These predictions significantly underestimate the Λ_c^+/D^0 ratio, although the prediction from PYTHIA 8 that includes additional color reconnection mechanisms [24] shows a p_T trend that is qualitatively similar to the measured trend. The CMS Collaboration has measured the Λ_c^+/D^0 ratio in pp collisions at $\sqrt{s} = 5.02$ TeV [28], which is consistent with predictions from PYTHIA 8 with additional color reconnection mechanisms. Λ_c^+ production was also measured by the LHCb Collaboration in pp collisions at $\sqrt{s} = 7$ TeV at forward rapidity [29], and the Λ_c^+/D^0 ratio was found to be lower than that measured by ALICE at midrapidity [14]. Calculations of the charm-hadron production cross section based on the k_T -factorization approach with gluon distributions obtained on the basis of novel collinear gluon distribution functions and Peterson fragmentation functions [30] are unable to simultaneously describe the ALICE and LHCb measurements using the same set of input parameters, suggesting that the measurements are difficult to explain within the independent parton fragmentation scheme. It is also important to note here that the magnitude of the relative production of Λ_b^0 baryons and beauty mesons in pp collisions measured by LHCb [31–33] and CMS [34] offer further hints that fragmentation fractions in the beauty sector differ between pp and e^+e^-/e^-p collisions.

Measurements in pp collisions also provide a necessary reference for studies in heavy-ion collisions, where the study

*Full author list given at the end of the article.

Published by the American Physical Society under the terms of the [Creative Commons Attribution 4.0 International](https://creativecommons.org/licenses/by/4.0/) license. Further distribution of this work must maintain attribution to the author(s) and the published article's title, journal citation, and DOI.

of charm production is a powerful tool to investigate the quark–gluon plasma (QGP) [35–37], the deconfined state of matter created under extreme energy densities. In particular, the charm baryon-to-meson ratio in heavy-ion collisions is sensitive to the charm hadronization mechanisms after the QGP phase. It is expected that a significant fraction of low- and intermediate-momentum charm quarks hadronize via recombination (coalescence) with light (anti)quarks from the medium [38,39], which would manifest as an enhancement of the Λ_c^+/D^0 ratio with respect to pp collisions. The Λ_c^+/D^0 ratio has been measured by STAR [40] in Au–Au collisions at $\sqrt{s_{\text{NN}}} = 200$ GeV, and by ALICE [41] and CMS [28] in Pb–Pb collisions at $\sqrt{s_{\text{NN}}} = 5.02$ TeV. These measurements offer constraints to different model calculations which implement contributions to hadronization via quark recombination [42–45].

The interpretation of the results obtained in heavy-ion collisions also requires detailed studies in p –Pb collisions to assess so-called cold nuclear matter (CNM) effects in the initial and final states, which could modify the production of heavy-flavor hadrons. In the initial state, the quark and gluon distributions are modified in bound nucleons compared to free nucleons, depending on the fractional longitudinal parton momentum x and the atomic mass number [46,47]. The most relevant CNM effect at LHC energies is shadowing, i.e., a decrease of the parton densities in the small- x region. This effect is due to high phase-space densities of low- x partons and can be described in collinear pQCD by means of parametrizations of the modification of the nuclear parton distribution functions (nPDFs) [48,49]. In the case of saturation of the parton phase-space, the color glass condensate (CGC) effective theory [50–54] offers an appropriate theoretical framework to describe the modification of the nPDFs. Moreover, partons can lose energy in the initial stages of the collisions due to initial-state radiation [55], or experience transverse momentum broadening due to multiple soft collisions before the heavy-quark pair is created in the hard scattering [56–58]. The modification of parton distributions in the nucleus and energy loss in the initial state can affect the yields and the momentum distributions of the produced hadrons, mainly at low momenta. In addition to initial-state effects, final-state effects such as hadronic rescattering [59] or the possible formation of a small QGP droplet [60,61] can also modify the hadron yields and momentum distributions. Several measurements in high-multiplicity pp and p –Pb collisions, such as long-range correlations of charged hadrons [62–65], and the enhancement of baryon-to-meson ratios in the light-flavor sector (p/π and Λ/K) [66–68], exhibit a similar behavior as that observed in Pb–Pb collisions, suggesting that these findings may have similar physical origins in pp , p –A, and A–A collisions [69]. Λ_c^+ production was previously measured at midrapidity by ALICE in p –Pb collisions at $\sqrt{s_{\text{NN}}} = 5.02$ TeV [14]. The Λ_c^+/D^0 ratio was found to be compatible within the uncertainties with that measured in pp collisions at $\sqrt{s} = 7$ TeV. The nuclear modification factor, $R_{p\text{Pb}}$, was found to be compatible with unity, as well as with models that implement cold nuclear matter effects via nPDF calculations [70] or assume the production of a deconfined medium in p –Pb collisions [60]. The LHCb Collaboration has measured the Λ_c^+/D^0 ratio at

forward rapidity in p –Pb collisions at $\sqrt{s_{\text{NN}}} = 5.02$ TeV [71] to be larger than that in pp collisions at forward rapidity [29] but smaller than the ALICE measurements in pp and p –Pb collisions at midrapidity [14].

Recent attempts have been made to model charm-baryon production in pp and p –Pb collisions. A framework based on a statistical hadronization model [72], which takes into account an increased set of charm-baryon states beyond those listed by the particle data group (PDG), is able to reproduce the Λ_c^+/D^0 ratios measured by ALICE in the pp and p –Pb collision systems, although it overestimates the LHCb measurement in pp collisions. A model implementing hadronization via recombination [73,74], where the p_T distributions of light and charm quarks and antiquarks are inputs of the model and the relative production of single-charm baryons to single-charm mesons is treated as a free parameter, is able to reproduce the p_T dependence of the Λ_c^+/D^0 ratio measured by ALICE at central rapidity in pp and p –Pb collisions, and by LHCb at forward rapidity in p –Pb collisions. While models implementing different approaches to Λ_c^+ production are effective in describing the measured Λ_c^+/D^0 ratio and $R_{p\text{Pb}}$, the large statistical and systematic uncertainties of the current measurements do not provide the discriminating power needed to differentiate between the various models. Therefore, more precise measurements are crucial to constrain predictions.

This paper presents the measurement of the p_T -differential production cross section of charm Λ_c^+ baryons in pp collisions in the rapidity interval $|y| < 0.5$ and in p –Pb collisions in $-0.96 < y < 0.04$ at $\sqrt{s_{\text{NN}}} = 5.02$ TeV, performed with the ALICE detector at the LHC. The rapidity y here and throughout this paper is defined in the center-of-mass system, and in p –Pb collisions the rapidity sign is positive in the p -going direction. The ratio of the production cross sections of Λ_c^+ baryons and D^0 mesons, Λ_c^+/D^0 , and the nuclear modification factor $R_{p\text{Pb}}$ are also presented. Finally, the Λ_c^+ production cross section per unit of rapidity at midrapidity is computed by integrating the p_T -differential Λ_c^+ production cross section after extrapolating down to $p_T = 0$, and the p_T -integrated Λ_c^+/D^0 ratios are presented. Two hadronic decay channels of Λ_c^+ were studied: $\Lambda_c^+ \rightarrow pK^-\pi^+$ and $\Lambda_c^+ \rightarrow pK_S^0$. Different analysis strategies were implemented, taking advantage of the methods used in previous analyses for the hadronic decays of D mesons [75–80] and Λ_c^+ baryons [14]. With respect to our previous measurement of Λ_c^+ production [14], the p_T reach was extended, the overall uncertainties of the measurements were reduced, and the analysis was performed in finer p_T intervals. The precision of the measurement of the nuclear modification factor $R_{p\text{Pb}}$ was improved with respect to the previously published result thanks to the larger data samples as well as a pp reference measured at the same center-of-mass energy.

The measurements are performed as the average of the particle and antiparticle cross sections, and so both Λ_c^+ and $\bar{\Lambda}_c^-$ baryons are referred to collectively as Λ_c^+ in the following. In all measurements the production cross section of prompt Λ_c^+ is reported, i.e., Λ_c^+ from direct hadronization of a charm quark or from decays of directly produced excited charm states. For the center-of-mass energy of pp collisions the simplified notation \sqrt{s} is used throughout this paper.

It is noted that the Λ_c^+/D^0 baryon-to-meson ratio is the focus of a dedicated letter [81], and this document presents a more detailed description of the analysis procedure as well as supplementary results.

II. EXPERIMENTAL SETUP AND DATA SAMPLES

The ALICE apparatus is composed of a central barrel, consisting of a set of detectors for particle reconstruction and identification covering the midrapidity region, a muon spectrometer at forward rapidity and various forward and backward detectors for triggering and event characterization. The central barrel detectors cover the full azimuth in the pseudorapidity interval $|\eta| < 0.9$ and are embedded in a large solenoidal magnet that provides a $B = 0.5$ T field parallel to the beam direction (z axis in the ALICE reference frame). A comprehensive description and overview of the typical performance of the detectors in pp and p -Pb collisions can be found in Refs. [82,83].

The tracking and particle identification capabilities of the ALICE central barrel detectors were exploited to reconstruct the Λ_c^+ decay products at midrapidity. The inner tracking system (ITS), consisting of three subdetectors, the silicon pixel detector (SPD), the silicon drift detector (SDD), and the silicon strip detector (SSD), each made of two concentric layers, allows for a precise determination of the track impact parameter (the distance of closest approach between the track and the primary vertex of the collision) in the transverse plane with a resolution better than $75 \mu\text{m}$ for tracks with $p_T > 1 \text{ GeV}/c$ [84]. The time projection chamber (TPC) is the main tracking detector of the experiment [85]. It provides up to 159 space points to reconstruct the charged-particle trajectory, and provides charged-particle identification (PID) via the measurement of the specific energy loss dE/dx . The particle identification capabilities are extended by the time-of-flight (TOF) detector, which is used to measure the flight time of charged particles from the interaction point. The TOF detector is an array of multigap resistive plate chambers. It measures the particle arrival time at the detector with a resolution of about 80 ps. The start time of the collision is obtained for each event either using the TOF detector, the T0 detector, or a combination of the two [86]. The T0 detector consists of two arrays of Cherenkov counters, located on both sides of the interaction point, covering the pseudorapidity regions $4.61 < \eta < 4.92$ and $-3.28 < \eta < -2.97$, respectively. The time resolution of the T0 detector in pp and p -Pb collisions is about 50 ps for events in which a measurement is made on both sides of the interaction point [86]. The V0 detector system, used for triggering and event selection, consists of two scintillator arrays covering the full azimuth in the pseudorapidity intervals $2.8 < \eta < 5.1$ and $-3.7 < \eta < -1.7$ ([82], Section 5.1). The zero degree calorimeter (ZDC), used for offline event rejection in p -Pb collisions, consists of two sets of neutron and proton calorimeters positioned along the beam axis on both sides of the ALICE apparatus, about 110 m from the interaction point ([82], Section 5.4).

The results presented in this paper were obtained from the analysis of the LHC Run 2 data samples collected from pp collisions at $\sqrt{s} = 5.02 \text{ TeV}$ in 2017 and p -Pb collisions

at $\sqrt{s_{NN}} = 5.02 \text{ TeV}$ in 2016. The proton–nucleon center-of-mass system in p -Pb collisions is shifted in rapidity by $\Delta y = 0.465$ in the Pb-going direction (negative rapidity) due to the asymmetric beam energies of 4 TeV for protons and 1.59 TeV per nucleon for Pb nuclei. The analyses used events recorded with a minimum bias (MB) trigger, which was based on coincident signals from the V0 detectors in both pp and p -Pb collisions. To remove background from beam–gas collisions and other machine-induced backgrounds, in pp collisions the events were further selected offline based on the correlation between the numbers of clusters and track segments reconstructed in the SPD, and V0 timing information. The latter was also used for the p -Pb analysis, together with the timing from the ZDC. To maintain a uniform ITS acceptance in pseudorapidity, only events with a z coordinate of the reconstructed vertex position within 10 cm from the nominal interaction point were analysed. Events with multiple interaction vertices due to pileup from several collisions were removed using an algorithm based on tracks reconstructed with the TPC and ITS detectors [83]. Using these selection criteria, approximately one billion MB-triggered pp events were analyzed, corresponding to an integrated luminosity of $\mathcal{L}_{\text{int}} = 19.5 \text{ nb}^{-1} (\pm 2.1\% [87])$, while approximately 600 million MB-triggered p -Pb events were selected, corresponding to $\mathcal{L}_{\text{int}} = 287 \mu\text{b}^{-1} (\pm 3.7\% [88])$.

III. Λ_c^+ ANALYSIS OVERVIEW AND METHODS

The analysis was performed using similar techniques to those reported in Ref. [14]. Λ_c^+ baryons were reconstructed in two hadronic decay channels: $\Lambda_c^+ \rightarrow pK^-\pi^+$ (branching ratio, $\text{BR} = 6.28 \pm 0.33\%$) and $\Lambda_c^+ \rightarrow pK_S^0$ ($\text{BR} = 1.59 \pm 0.08\%$), followed by the subsequent decay $K_S^0 \rightarrow \pi^+\pi^-$ ($\text{BR} = 69.2 \pm 0.05\%$) [89]. For the former, the Λ_c^+ decays to the $pK^-\pi^+$ final state via four channels: $\Lambda_c^+ \rightarrow p\bar{K}^{*0}(892)$, $\Lambda_c^+ \rightarrow \Delta^{++}(1232)K^-$, $\Lambda_c^+ \rightarrow \Lambda(1520)\pi^+$, and the nonresonant $\Lambda_c^+ \rightarrow pK^-\pi^+$ decay. As these channels are indistinguishable in the analysis, all four are considered together.

The selection of candidates was performed using a combination of kinematical, geometrical, and PID selections. The selection criteria were tuned on Monte Carlo simulations to maximize the statistical significance in each p_T interval. Λ_c^+ candidates were reconstructed by combining reconstructed tracks with $|\eta| < 0.8$ and at least 70 reconstructed space points in the TPC. For all decay products in the $\Lambda_c^+ \rightarrow pK^-\pi^+$ analysis and for the proton-candidate tracks in the $\Lambda_c^+ \rightarrow pK_S^0$ analysis, at least one cluster was required in either of the two SPD layers. The PID selections for all analyses were performed utilising the Bayesian method for combining the TPC and TOF signals, as described in Ref. [90]. The Bayesian method entails the use of priors, an *a priori* probability of measuring a given particle species, which are determined using measured particle abundances. Where possible, the TPC and TOF signals were combined; however, if the TOF signal was absent for a given track, the TPC signal alone was used. For the $\Lambda_c^+ \rightarrow pK_S^0$ analysis in p -Pb collisions, a machine learning approach with boosted decision

trees (BDTs) was applied to select Λ_c^+ candidates, using the toolkit for multivariate data analysis (TMVA) [91].

The detector acceptance for Λ_c^+ baryons varies as a function of rapidity, in particular falling steeply to zero for $|y| > 0.5$ at low p_T , and $|y| > 0.8$ for $p_T > 5$ GeV/c. For this reason, a fiducial acceptance selection was applied on the rapidity of candidates, $|y_{\text{lab}}| < y_{\text{fid}}(p_T)$, where y_{fid} increases smoothly from 0.5 to 0.8 in $0 < p_T < 5$ GeV/c and $y_{\text{fid}} = 0.8$ for $p_T > 5$ GeV/c [75].

For the $\Lambda_c^+ \rightarrow pK^-\pi^+$ analysis, candidates were formed by combining triplets of tracks with the correct configuration of charge sign. For this decay channel, the high-resolution tracking and vertexing information provided by the ITS and TPC allows the interaction point (primary vertex) and the reconstructed decay point of the Λ_c^+ candidate (secondary vertex) to be distinguished from one another, despite the short decay length of the Λ_c^+ ($c\tau = 60.7 \mu\text{m}$ [89]). Once the secondary vertex was computed from the three tracks forming the Λ_c^+ candidate, selections were applied on variables related to the kinematic properties of the decay, the quality of the reconstructed vertex, and the displaced decay-vertex topology. These variables comprise the transverse momenta of the decay products; the quadratic sum of the distance of closest approach of each track to the secondary vertex; the decay length of the Λ_c^+ candidate (separation between the primary and secondary vertices); and the cosine of the pointing angle between the Λ_c^+ candidate flight line (the vector that connects the primary and secondary vertices) and the reconstructed momentum vector of the candidate. Pions, kaons, and protons were identified using the *maximum-probability* Bayesian PID approach [90], where a probability is assigned to each track for every possible species based on the TPC and TOF signals and the identity of the track is taken to be the species with the highest probability value. This approach allows for a higher-purity sample to be selected, reducing the large level of combinatorial background and facilitating the signal extraction.

The $\Lambda_c^+ \rightarrow pK_S^0$ analysis started from a $K_S^0 \rightarrow \pi^+\pi^-$ candidate, which is reconstructed as a pair of opposite-sign charged tracks forming a neutral decay vertex displaced from the primary vertex (a V^0 candidate). This V^0 candidate was paired with a proton-candidate track originating from the primary vertex to form a Λ_c^+ candidate. Two strategies were then used to select Λ_c^+ candidates in pp and p -Pb collisions. In pp collisions, the analysis was based on rectangular selection criteria. The V^0 candidate was required to have an invariant mass compatible with the K_S^0 mass from the PDG [89] within $8(20) \text{ MeV}/c^2$ at low (high) p_T , corresponding to one or two times the resolution of the K_S^0 invariant mass, depending on the p_T interval and the collision system. The V^0 candidates were selected based on the p_T and impact parameter of the decay pions to the K_S^0 decay vertex, and the cosine of the pointing angle between the V^0 flight line and its reconstructed momentum. Proton-candidate tracks were selected based on their p_T , their impact parameter to the primary vertex, the number of reconstructed TPC clusters, and a cluster being present on at least one of the two SPD layers. Particle identification was performed on the proton-candidate track, first using a loose $|n_\sigma| < 3$ preselection on the TPC response,

where n_σ corresponds to the difference between the measured and expected dE/dx for a given particle species, in units of the resolution. This was followed by a strict requirement that the Bayesian posterior probability for the track to be a proton must be greater than 80%.

In p -Pb collisions, an approach using BDTs was used for the $\Lambda_c^+ \rightarrow pK_S^0$ decay. The BDT algorithm provides a classification tree that maps simulated Λ_c^+ candidates to a single BDT response variable aiming to maximize the separation between signal and background candidates. The mapping function is then applied on a real data sample in which the true identities of particles are unknown, followed by the application of selections on the BDT response. Candidates were initially filtered using an $|n_\sigma^{\text{TPC}}| < 3$ PID selection on the proton candidate. Independent BDTs were trained for each p_T interval in the analysis. The training was performed on samples of simulated events including a detailed description of the experimental apparatus and the detector response. The training sample for signal candidates was taken from a simulation of pp events containing charm hadrons generated using PYTHIA 6.4.25 [92] with the Perugia2011 tune [93], embedded into an underlying p -Pb collision generated with HIJING 1.36 [94]. The background candidates were taken from the HIJING simulation. The variables that were used in the training were the Bayesian PID probability of the proton-candidate track to be a proton, the p_T of the proton candidate, the invariant mass and $c\tau$ of the K_S^0 candidate, and the impact parameters of the V^0 and the proton-candidate track with respect to the primary vertex. The MC samples used for the efficiency calculation were different from those used in the training. The selection on the BDT response was tuned in each p_T interval to maximize the expected statistical significance, which is estimated using (i) the signal obtained from the generated Λ_c^+ yield multiplied by the selection efficiency of the trained model and (ii) the background estimated from preselected data multiplied by the background rejection factor from the BDT. The BDT analysis was cross checked with an independent analysis using rectangular selection criteria, and the two results were found to be fully consistent within the experimental uncertainties.

Signal extraction for all analyses was performed by means of a fit to the invariant mass distributions of candidates in each p_T interval under study. A Gaussian function was used to model the signal peak and an exponential or polynomial function was used to model the background. Due to the small signal-to-background ratio, the standard deviation of the Gaussian signal function was fixed to the value obtained from simulations to improve the fit stability. In pp collisions, a Λ_c^+ signal could be extracted for the $\Lambda_c^+ \rightarrow pK^-\pi^+$ and $\Lambda_c^+ \rightarrow pK_S^0$ analyses in the range $1 < p_T < 12$ GeV. In p -Pb collisions a Λ_c^+ signal was extracted for the $\Lambda_c^+ \rightarrow pK_S^0$ analysis in the range $1 < p_T < 24$ GeV/c, and for the $\Lambda_c^+ \rightarrow pK^-\pi^+$ analysis in the range $2 < p_T < 24$ GeV/c, as the larger combinatorial background in the $\Lambda_c^+ \rightarrow pK^-\pi^+$ channel limits the low- p_T reach. A selection of the invariant mass distributions with their corresponding fit functions is displayed in Fig. 1 for different p_T intervals, decay channels, and collision systems.

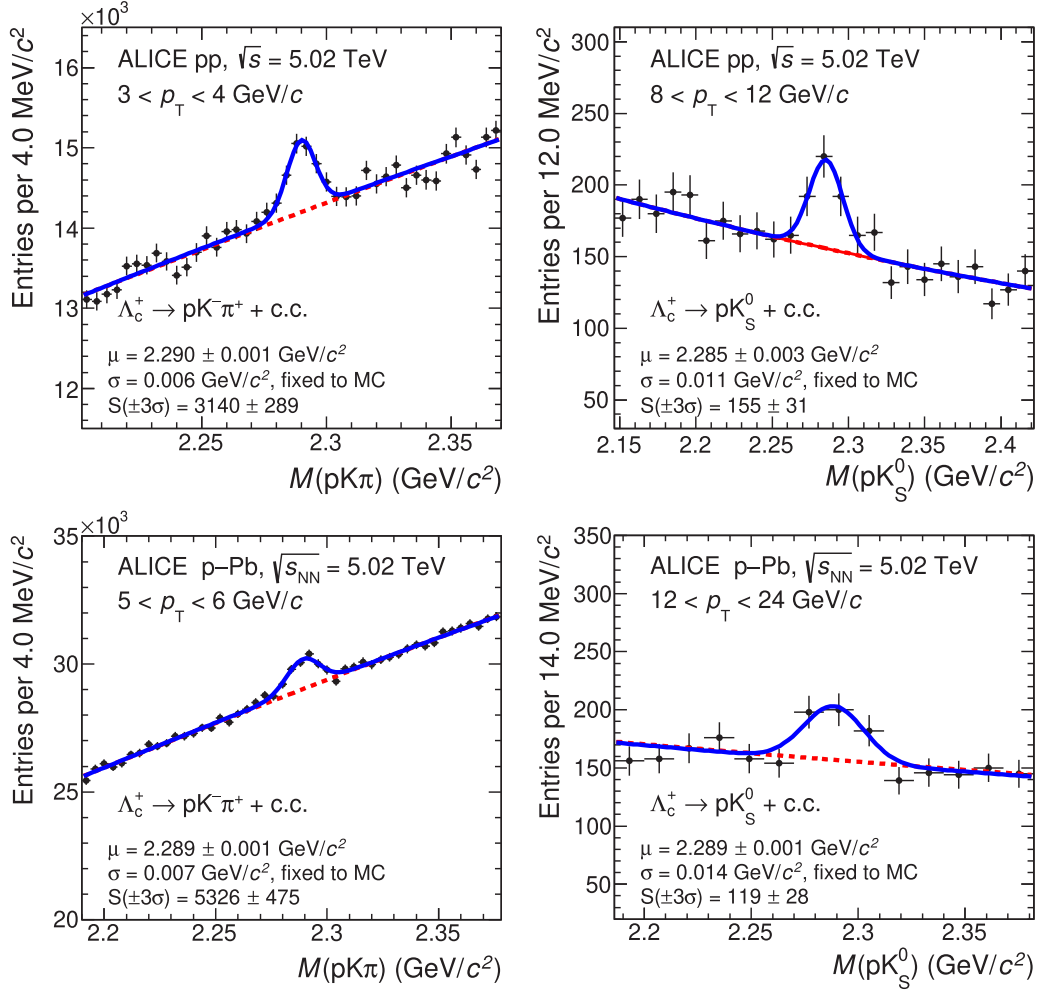


FIG. 1. Invariant mass distributions of Λ_c^+ candidates in different p_T intervals, collision systems, and decay channels, with the corresponding fit functions. Top-left: $\Lambda_c^+ \rightarrow pK^-\pi^+$ for $3 < p_T < 4$ GeV/c in pp collisions; top-right: $\Lambda_c^+ \rightarrow pK_S^0$ for $8 < p_T < 12$ GeV/c in pp collisions; bottom-left: $\Lambda_c^+ \rightarrow pK^-\pi^+$ for $5 < p_T < 6$ GeV/c in p -Pb collisions; bottom-right: $\Lambda_c^+ \rightarrow pK_S^0$ with BDT analysis in $12 < p_T < 24$ GeV/c in p -Pb collisions. The dashed lines represent the fit to the background and the solid lines represent the total fit function.

IV. CORRECTIONS

The p_T -differential cross section of prompt Λ_c^+ -baryon production was obtained for each decay channel as

$$\frac{d^2\sigma^{\Lambda_c^+}}{dp_T dy} = \frac{1}{2c_{\Delta y} \times \Delta p_T} \times \frac{1}{\text{BR}} \times \frac{f_{\text{prompt}} \times N_{|y| < y_{\text{fid}}}^{\Lambda_c^+}}{(A \times \epsilon)_{\text{prompt}}} \times \frac{1}{\mathcal{L}_{\text{int}}}, \quad (1)$$

where $N^{\Lambda_c^+}$ is the raw yield (sum of particles and antiparticles) in a given p_T interval with width Δp_T , f_{prompt} is the fraction of the raw yield from prompt Λ_c^+ , BR is the branching ratio for the considered decay mode, and \mathcal{L}_{int} is the integrated luminosity. $(A \times \epsilon)$ is the product of detector acceptance and efficiency for prompt Λ_c^+ baryons, where ϵ accounts for the reconstruction of the collision vertex, the reconstruction and selection of the tracks of the Λ_c^+ decay products, and the Λ_c^+ -candidate selection. The correction factor for the rapidity coverage, $c_{\Delta y}$, was computed as the ratio between the generated Λ_c^+ -baryon yield in $|y_{\text{lab}}| < y_{\text{fid}}(p_T)$ and that in $|y_{\text{lab}}| < 0.5$, where the Λ_c^+ -baryon rapidity shape was taken from FONLL pQCD calculations. The factor 2 in the denominator

of Eq. (1) takes into account that the raw yield includes both particles and antiparticles, while the cross section is given for particles only and is computed as the average of Λ_c^+ and $\bar{\Lambda}_c^-$.

The correction factor $(A \times \epsilon)$ was obtained following the same approach as discussed in Ref. [78]. The correction factors were obtained from simulations in which the detector and data taking conditions of the corresponding data samples were reproduced. PYTHIA 6.4.25 and PYTHIA 8.243 [95] were used to simulate pp collisions. For p -Pb collisions, a pp event containing heavy-flavor signals was generated with PYTHIA 6 and HIJING was used to simulate the underlying background event.

The $(A \times \epsilon)$ was computed separately for prompt and non-prompt Λ_c^+ . The $\Lambda_c^+ \rightarrow pK^-\pi^+$ decay channel includes not only the direct (nonresonant) decay mode but also three resonant channels, as explained in Sec. III. Due to the kinematical properties of these decays, the acceptance and efficiency of each decay mode is different and the final correction was determined as a weighted average of the $(A \times \epsilon)$ values of the four decay channels with the relative branching ratios as weights.

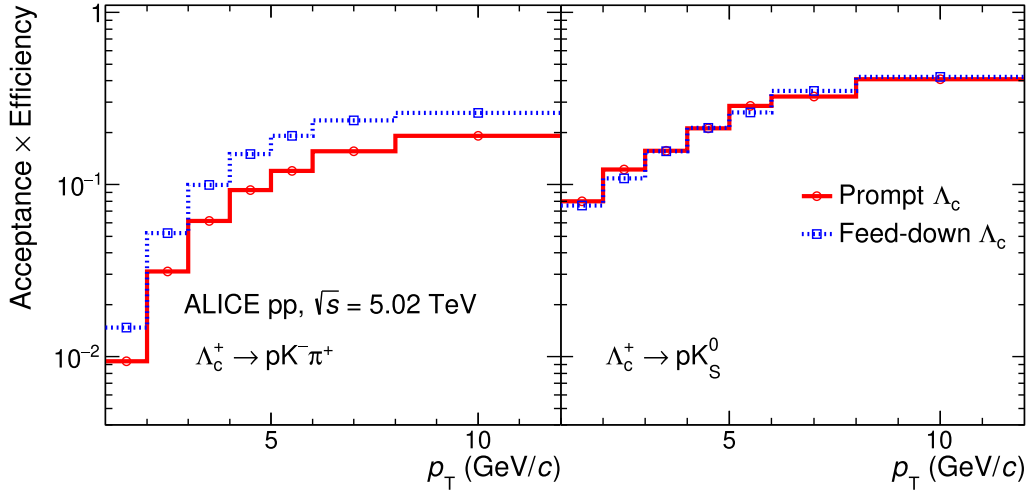


FIG. 2. Product of detector acceptance and efficiency for Λ_c^+ baryons in pp collisions at $\sqrt{s} = 5.02$ TeV, as a function of p_T . From left to right: $\Lambda_c^+ \rightarrow pK^-\pi^+$ and $\Lambda_c^+ \rightarrow pK_S^0$. The solid lines correspond to the $(A \times \epsilon)$ for prompt Λ_c^+ , while the dotted lines represent $(A \times \epsilon)$ for Λ_c^+ baryons originating from beauty-hadron decays. The statistical uncertainties are smaller than the marker size.

Figures 2 and 3 show the product of $(A \times \epsilon)$ for Λ_c^+ baryons with $|y| < y_{\text{fid}}$ in pp and p -Pb collisions as a function of p_T for the $\Lambda_c^+ \rightarrow pK^-\pi^+$ (left panel) and $\Lambda_c^+ \rightarrow pK_S^0$ (right panel) decay channels. The higher $(A \times \epsilon)$ for Λ_c^+ from beauty-hadron decays in the $\Lambda_c^+ \rightarrow pK^-\pi^+$ decay channel is due to the geometrical selections on the displaced decay-vertex topology, which enhance the nonprompt component because of the relatively longer lifetime of the beauty hadrons compared to prompt Λ_c^+ . For the $\Lambda_c^+ \rightarrow pK_S^0$ analyses, the $(A \times \epsilon)$ of prompt and nonprompt Λ_c^+ are compatible, as selections based on the displaced decay-vertex topology are not applied.

Contrary to pp collisions, where the charged-particle multiplicity in data is well described by the simulation, in p -Pb collisions a weighting procedure based on the event multiplicity was used in the calculation of the reconstruction efficiency from the simulated events. This approach accounts for the

dependence of the reconstruction efficiency on the event multiplicity, which is due to the fact that the resolutions of the primary-vertex position and of the variables used in the geometrical selections of displaced decay vertices improve with increasing multiplicity. The event multiplicity was defined here using the number of tracklets, where a tracklet is defined as a track segment joining the reconstructed primary vertex with a space point on each SPD layer within the pseudorapidity range $|\eta| < 1.0$.

The factor f_{prompt} was calculated as in Ref. [14]:

$$\begin{aligned}
 f_{\text{prompt}} &= 1 - \frac{N^{\Lambda_c, \text{feed-down}}}{N^{\Lambda_c}} \\
 &= 1 - \frac{(A \times \epsilon)_{\text{feed-down}} c_{\Delta y} \Delta p_T \text{BR} \mathcal{L}_{\text{int}}}{N^{\Lambda_c}/2} \\
 &\quad \times \left(\frac{d^2\sigma}{dp_T dy} \right)_{\text{feed-down}}^{\text{FONLL}}, \quad (2)
 \end{aligned}$$

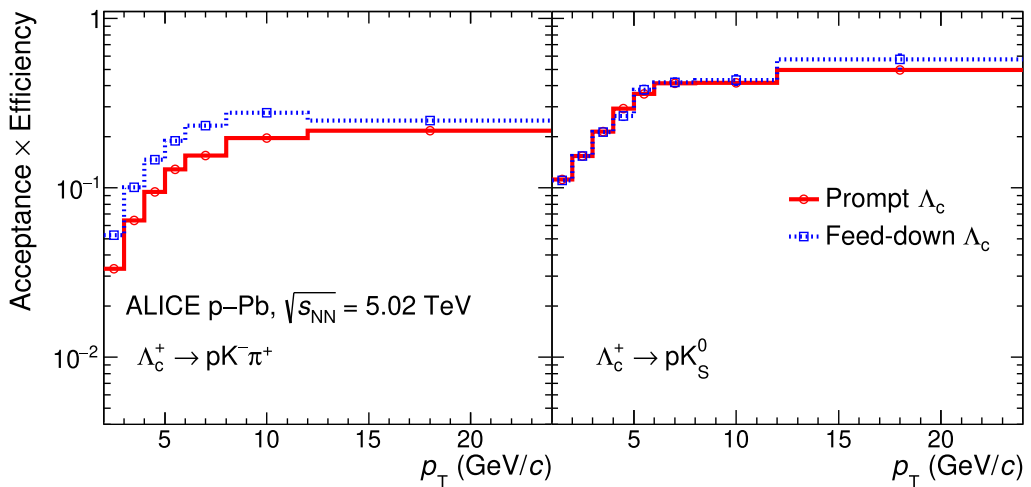


FIG. 3. Product of detector acceptance and efficiency for Λ_c^+ baryons in p -Pb collisions at $\sqrt{s_{\text{NN}}} = 5.02$ TeV, as a function of p_T . From left to right: $\Lambda_c^+ \rightarrow pK^-\pi^+$ and $\Lambda_c^+ \rightarrow pK_S^0$. The solid lines correspond to the $(A \times \epsilon)$ for prompt Λ_c^+ , while the dotted lines represent $(A \times \epsilon)$ for Λ_c^+ baryons originating from beauty-hadron decays. The statistical uncertainties are smaller than the marker size.

TABLE I. Summary of the systematic uncertainties for the two Λ_c^+ decay modes in pp collisions at $\sqrt{s} = 5.02$ TeV. The uncertainty sources found to be $<1\%$ were considered negligible (“negl.” in the table).

	$\Lambda_c^+ \rightarrow pK^-\pi^+$		$\Lambda_c^+ \rightarrow pK_S^0$	
	Lowest p_T	Highest p_T	Lowest p_T	Highest p_T
Yield extraction (%)	10	8	8	7
Tracking efficiency (%)	6	7	3	5
Selection efficiency (%)	6	6	3	3
PID efficiency (%)	5	5	2	4
MC p_T shape (%)	negl.	negl.	negl.	negl.
$(A \times \varepsilon)$ stat. unc. (%)	1.7	1.8	1.7	3.5
Beauty feed-down (%)	+1.1 -1.8	+5.3 -8.0	+0.8 -1.3	+2.6 -4.0
Branching ratio (%)	5.1		5.0	
Luminosity (%)	2.1			

where $N^{\Lambda_c}/2$ is the raw yield divided by a factor of two to account for particles and antiparticles. The production cross section of Λ_c^+ from beauty-hadron decays, $(\frac{d^2\sigma}{dp_T dy})_{\text{feed-down}}^{\text{FONLL}}$, was calculated using the b-quark p_T -differential cross section from FONLL calculations [12,13], the fraction of beauty quarks that fragment into beauty hadrons H_b estimated from LHCb measurements [33], and the $H_b \rightarrow \Lambda_c^+ + X$ decay kinematics and branching ratios of $f(H_b \rightarrow \Lambda_c^+ + X)$ modelled using PYTHIA 8 simulations [95].

The beauty-hadron fragmentation was derived from the LHCb measurements of the \bar{B}_s^0 - and Λ_b^0 -production fraction relative to \bar{B}^0 and B^- mesons in pp collisions at $\sqrt{s} = 13$ TeV [33], which indicates that the fraction of b quarks hadronizing into a Λ_b^0 baryon is strongly p_T -dependent in the measured range of $4 < p_T < 25$ GeV/ c . The fits to the production fractions of \bar{B}_s^0 and Λ_b^0 hadrons normalized to the sum of B^- and \bar{B}^0 hadrons are presented in Ref. [33] as a function of the beauty-hadron p_T as

$$\frac{f_s}{f_u + f_d}(p_T) = A[p_1 + p_2 \times (p_T - \langle p_T \rangle)] = X, \quad (3)$$

$$\frac{f_{\Lambda_b^0}}{f_u + f_d}(p_T) = C[q_1 + \exp(q_2 + q_3 \times p_T)] = Y, \quad (4)$$

where f_u , f_d , f_s , and $f_{\Lambda_b^0}$ are the fractions of b quarks that hadronize into \bar{B}^0 , B^- , \bar{B}_s^0 , and Λ_b^0 , respectively, and A , p_1 , p_2 , $\langle p_T \rangle$, C , q_1 , q_2 , and q_3 are free parameters of the fits to the measured ratios. The beauty hadron fragmentation fractions are defined assuming $f_u = f_d$ and $f_u + f_d + f_s + f_{\Lambda_b^0} = 1$. Around 90% of the feed-down Λ_c^+ comes from $\Lambda_b^0 \rightarrow \Lambda_c^+ + X$ decays, and the Λ_b^0 fragmentation fraction can be defined as

$$f_{\Lambda_b^0}(p_T) = \frac{Y}{(X + Y + 1)}. \quad (5)$$

For $p_T = 5$ GeV/ c , $f_{\Lambda_b^0}$ is around 0.2, and it decreases to a value of around 0.09 for $p_T > 20$ GeV/ c . For $p_T < 5$ GeV/ c it was assumed that $f_{\Lambda_b^0} = 0.2$, since measurements of the ratio Λ_b^0/\bar{B}^0 in pp collisions at $\sqrt{s} = 7$ TeV and 8 TeV [32] are flat as a function of p_T in this interval within the experimental uncertainties. It was assumed that there is no rapidity dependence of $f_{\Lambda_b^0}$ since the LHCb measurements of

beauty-production ratios are flat as a function of rapidity in $2 < y < 5$ within the experimental uncertainties [32,33].

For p -Pb collisions, a hypothesis on the nuclear modification factor $R_{p\text{Pb}}^{\text{feed-down}}$ of Λ_c^+ from beauty-hadron decays was included as an additional factor in the last term of Eq. (2). As in the D -meson analyses [76], it was assumed that the $R_{p\text{Pb}}$ of prompt and feed-down Λ_c^+ are equal. The values of f_{prompt} in both collision systems range between 87% and 98% for the $\Lambda_c^+ \rightarrow pK_S^0$ decay channel and between 84% and 98% for the $\Lambda_c^+ \rightarrow pK^-\pi^+$ decay channel.

V. EVALUATION OF SYSTEMATIC UNCERTAINTIES

This section describes the various sources of systematic uncertainties of the measured cross section in each analysis and the methods used to estimate them. A summary of the systematic uncertainties is shown in Tables I and II for the pp and p -Pb analyses, respectively. The different sources of systematic uncertainty are assumed to be uncorrelated, and their contributions are added in quadrature to calculate the overall systematic uncertainty in each p_T interval.

The systematic uncertainty on the yield extraction was estimated by repeating the fits to the invariant mass distributions several times, varying (i) the lower and upper limits of the fit interval and (ii) the functional form of the background (linear, exponential, and second-order polynomial functions were used). For each of the above trials, the fit was repeated with different hypotheses on the signal peak width and mean, with variations including (a) treating both the Gaussian width and mean as free parameters, (b) fixing the peak width to the MC expectation and leaving the mean free, (c) fixing the mean to the MC expectation and leaving the peak width free, and (d) fixing both the peak width and mean to the MC expectation. The systematic uncertainty was defined as the RMS of the distribution of the raw yield values extracted from these trials.

The systematic uncertainty on the tracking efficiency was estimated by (i) comparing the probability of prolonging a track from the TPC to the ITS (“matching efficiency”) in data and simulation and (ii) varying track selection criteria in the analyses. The matching efficiency in simulation was determined after reweighting the relative abundance of primary and secondary particles to match that in data. The uncertainty on

TABLE II. Summary of the systematic uncertainties for the two Λ_c^+ decay modes in p -Pb collisions at $\sqrt{s_{\text{NN}}} = 5.02$ TeV. The uncertainty sources found to be $<1\%$ were considered negligible (“negl.” in the table).

	$\Lambda_c^+ \rightarrow pK^-\pi^+$		$\Lambda_c^+ \rightarrow pK_S^0$	
	Lowest p_T	Highest p_T	Lowest p_T	Highest p_T
Yield extraction (%)	8	10	10	8
Tracking efficiency (%)	6	6	6	5
Selection efficiency (%)	10	6	15	8
PID efficiency (%)	5	5	negl.	negl.
MC p_T shape (%)	1	1	1	1
$(A \times \varepsilon)$ stat. unc. (%)	1.1	4.0	0.5	3.0
Beauty feed-down (%)	+1.8 -3.0	+4.2 -6.7	+0.9 -1.5	+4.6 -7.0
Branching ratio (%)	5.1		5.0	
Luminosity (%)	3.7			

the matching efficiency was defined as the relative difference in the matching efficiency between simulation and data. It is species-dependent and therefore it was determined individually for protons, kaons, and pions. In the $\Lambda_c^+ \rightarrow pK_S^0$ analysis only the proton matching efficiency uncertainty was included since no ITS condition was required for the pion tracks from the K_S^0 decay. The per-track uncertainty on the matching efficiency is p_T dependent and it was propagated to the Λ_c^+ taking into account the decay kinematics and treating the uncertainty as correlated among the tracks. The second contribution to the track reconstruction uncertainty was estimated by repeating the analysis varying the TPC track selection criteria. The uncertainty was defined as the RMS of the Λ_c^+ cross section values obtained with the different track selections. The total uncertainty on the tracking efficiency was defined as the quadratic sum of these two contributions.

The uncertainty on the Λ_c^+ selection efficiency due to imperfections in the simulated kinematical and geometrical variables used to select Λ_c^+ candidates was estimated by varying the selection criteria. For the BDT analysis in the $\Lambda_c^+ \rightarrow pK_S^0$ channel, variations were made on the selection of the BDT response. The systematic uncertainty was estimated in each p_T interval as the RMS of the distribution of the corrected cross section values resulting from these variations.

Systematic uncertainties can arise from discrepancies in the PID efficiency between simulation and data. In the case of the $\Lambda_c^+ \rightarrow pK_S^0$ analysis in pp collisions, the systematic uncertainty associated with the PID efficiency was estimated by varying the minimum probability threshold required to identify a track as a proton. For the $\Lambda_c^+ \rightarrow pK^-\pi^+$ analysis, the systematic uncertainty was estimated by applying a minimum threshold selection on the Bayesian probability to assign the track identity, with the threshold varying between 30% and 80%. The systematic uncertainty in both cases was defined based on the variation of the corrected cross section. For the $\Lambda_c^+ \rightarrow pK_S^0$ analysis in p -Pb collisions, the PID variables were included as part of the BDT, and therefore the PID uncertainty is already accounted for by varying the selection on the BDT response. The contribution due to the 3σ PID preselection was found to be negligible.

An additional source of systematic uncertainty was assigned due to the dependence of the efficiencies on the generated p_T distribution of Λ_c^+ in the simulation (“MC p_T shape” in Tables I and II). To estimate this effect the efficiencies were evaluated after reweighting the p_T shape of the PYTHIA 6 simulations to match the p_T spectrum of D mesons from FONLL pQCD calculations. An uncertainty was assigned in each p_T interval based on the difference between the central and reweighted efficiencies.

The relative statistical uncertainty on $(A \times \varepsilon)$ was considered as an additional systematic uncertainty source, originating from the finite statistics in the simulation used to calculate the efficiency.

The systematic uncertainty on the prompt fraction (“Beauty feed-down” in Tables I and II) was estimated by varying independently (i) the production cross section of beauty quarks within the theoretical uncertainties in FONLL [13] and (ii) the function describing the fragmentation fraction $f_{\Lambda_b^0}$. For the variation of (ii), the free parameters defined in Ref. [33] were varied independently within their uncertainties. For $p_T(\Lambda_b^0) < 5$ GeV/c, the lower uncertainty bound of $f_{\Lambda_b^0}$ was taken to be equal to the lower bound of the fit at $p_T(\Lambda_b^0) = 5$ GeV/c, independent of p_T , while the upper uncertainty bound was taken to be equal to the p_T -dependent upper bound of the fit. To account for a possible \sqrt{s} dependence of the fragmentation fractions, an additional reduction of the lower bound of $f_{\Lambda_b^0}$ was considered based on the spread of the LHCb measurements at different values of \sqrt{s} . In the p -Pb analyses the uncertainty on the hypothesis of the nuclear modification factor of Λ_c^+ from beauty-hadron decays was estimated by varying the ratio $R_{pPb}^{\text{feed-down}}/R_{pPb}^{\text{prompt}}$ in the range $0.9 < R_{pPb}^{\text{feed-down}}/R_{pPb}^{\text{prompt}} < 1.3$. This range was chosen based on theoretical calculations of charm and beauty hadron production in p -Pb collisions as explained in Ref. [76]. The overall uncertainty on the prompt fraction was defined as the envelope of these variations, which leads to an asymmetric uncertainty.

The uncertainty on the luminosity measurement is 2.1% for pp collisions [87] and 3.7% for p -Pb collisions [88]. The uncertainty on the branching fractions are 5.1% for the $\Lambda_c^+ \rightarrow pK^-\pi^+$ channel, and 5.0% for the $\Lambda_c^+ \rightarrow pK_S^0$ channel [89].

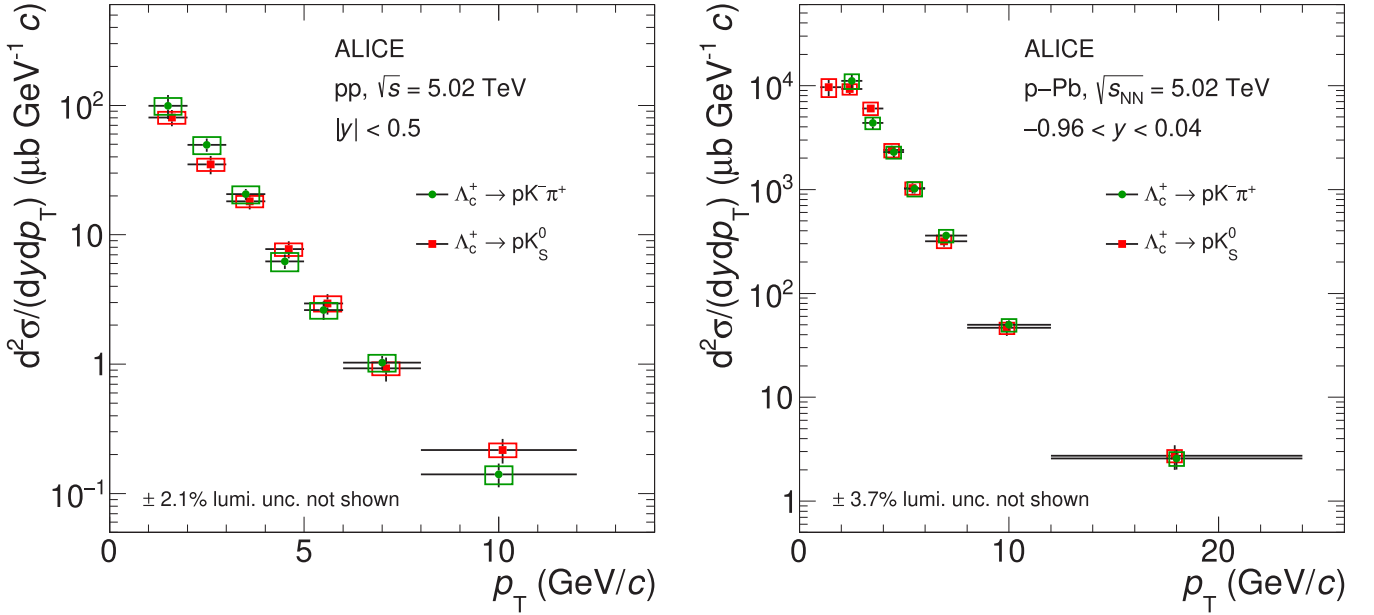


FIG. 4. Left: p_T -differential prompt Λ_c^+ -baryon cross section in pp collisions at $\sqrt{s} = 5.02$ TeV in the interval $1 < p_T < 12$ GeV/c. Right: p_T -differential prompt Λ_c^+ -baryon cross section in p -Pb collisions at $\sqrt{s_{NN}} = 5.02$ TeV in the interval $1 < p_T < 24$ GeV/c. The statistical uncertainties are shown as vertical bars and the systematic uncertainties are shown as boxes. Horizontal position of points are shifted to provide better visibility.

VI. RESULTS

A. p_T -differential cross sections

The p_T -differential cross section of prompt Λ_c^+ -baryon production in pp collisions at $\sqrt{s} = 5.02$ TeV, measured in the rapidity interval $|y| < 0.5$ and p_T interval $1 < p_T < 12$ GeV/c, is shown in Fig. 4 (left) for the two decay channels $\Lambda_c^+ \rightarrow pK^-\pi^+$ and $\Lambda_c^+ \rightarrow pK_S^0$. Figure 4 (right) shows the p_T -differential cross section of prompt Λ_c^+ -baryon production in p -Pb collisions at $\sqrt{s_{NN}} = 5.02$ TeV, measured in the rapidity interval $-0.96 < y < 0.04$ and p_T interval $1 < p_T < 24$ GeV/c for the two decay channels $\Lambda_c^+ \rightarrow pK^-\pi^+$ and $\Lambda_c^+ \rightarrow pK_S^0$. The measurements in the different decay channels agree within statistical and uncorrelated systematic uncertainties, with the largest discrepancies among the measured values being smaller than 1.4σ .

To obtain a more precise measurement of the p_T -differential Λ_c^+ -baryon production cross section, the results from the two decay channels were combined, taking into account the correlation between the statistical and systematic uncertainties. The systematic uncertainties treated as uncorrelated between the different decay channels ($\Lambda_c^+ \rightarrow pK^-\pi^+$ and $\Lambda_c^+ \rightarrow pK_S^0$) include those due to the raw-yield extraction, the Λ_c^+ -selection efficiency, and the $(A \times \epsilon)$ statistical uncertainties. The systematic uncertainties due to the tracking efficiency, the PID efficiency, the generated Λ_c^+ p_T spectrum, the beauty feed-down, and the luminosity were treated as correlated between the two decay channels. The branching ratio uncertainties were considered to be partially correlated, as described in Ref. [89]. A weighted average of the cross section values obtained from the different analyses was calculated, using the inverse of the quadratic sum of the relative statistical and uncorrelated systematic uncertainties as weights.

Figure 5 shows the measured production cross section (average of the two decay channels) in pp collisions compared to predictions from MC generators and pQCD calculations. The left panel shows the comparison with predictions from different tunes of the PYTHIA 8 generator, including the Monash tune [23], and tunes that implement color reconnection (CR) beyond the leading-color approximation [24]. These additional color reconnection topologies include “junctions” which fragment into baryons, leading to increased baryon production. For the CR tunes, three modes are considered (Modes 0, 2, and 3), as described in Ref. [24], which apply different constraints on the allowed reconnection, taking into account causal connection of dipoles involved in a reconnection and time-dilation effects caused by relative boosts between string pieces. It is noted that Mode 2 is recommended in Ref. [24] as the standard tune, and contains the strictest constraints on the allowed reconnection. In the simulations with the three CR modes, all soft QCD processes are switched on. All PYTHIA 8 tunes underestimate the measured p_T -differential prompt Λ_c^+ cross section. The Monash tune significantly underestimates the cross section by a factor ~ 12 for $1 < p_T < 2$ GeV/c, and around a factor 2–3 for $p_T > 5$ GeV/c. All three CR modes yield a similar magnitude and shape of the Λ_c^+ cross section, and predict a significantly larger Λ_c^+ production cross section with respect to the Monash tune. However, for all three CR modes, the measured Λ_c^+ production cross section is underestimated by a factor of about two for $1 < p_T < 2$ GeV/c. For $p_T > 5$ GeV/c, Mode 2 and Mode 3 provide a good description of the data, while Mode 0 underestimates the data by 15–20%. All tunes exhibit a harder p_T distribution than observed in data.

The right panel of Fig. 5 shows a comparison with a NLO pQCD calculation obtained with the POWHEG frame-

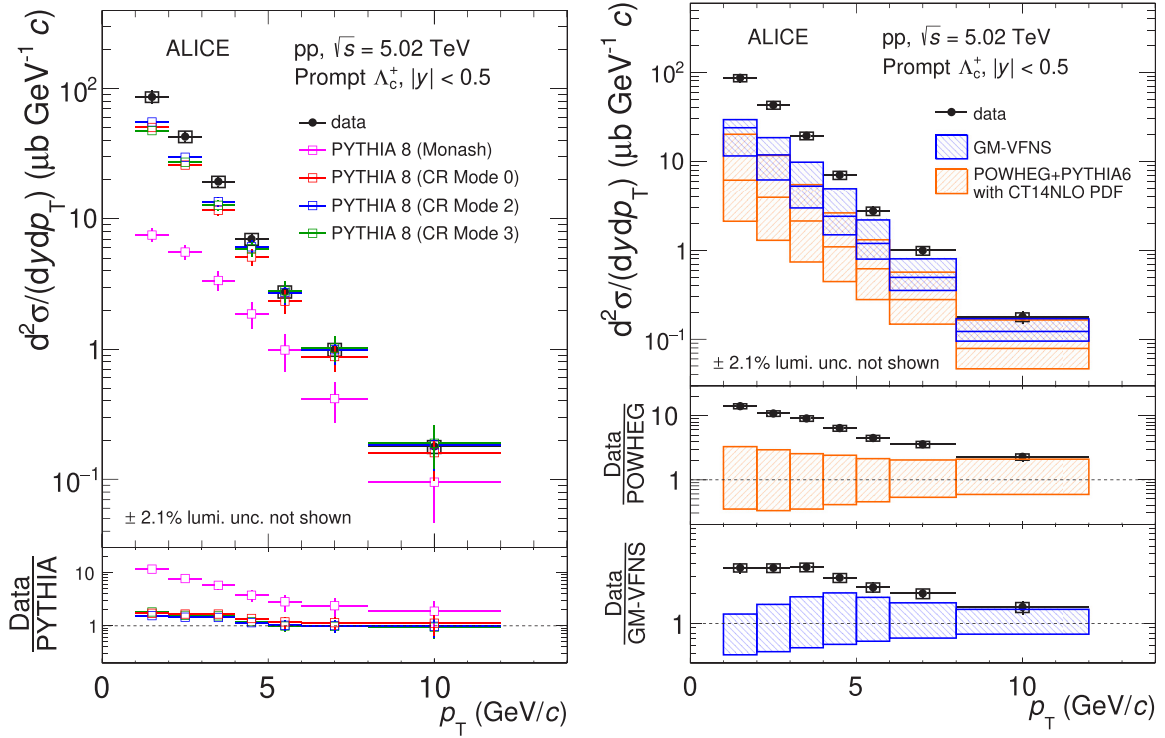


FIG. 5. Prompt Λ_c^+ -baryon p_T -differential production cross section in pp collisions at $\sqrt{s} = 5.02$ TeV in the interval $1 < p_T < 12$ GeV/ c . The statistical uncertainties are shown as vertical bars and the systematic uncertainties are shown as boxes. Left: Comparison to predictions from different tunes of the PYTHIA 8 event generator [23,24]. The vertical bars on the PYTHIA 8 predictions represent the statistical uncertainty from the simulation, and the vertical bars on the ratios in the bottom panel also include the statistical uncertainties from the data. Right: Comparison to predictions from the POWHEG event generator [96] and GM-VFNS calculations [98]. The orange(blue) boxes represent the uncertainties of POWHEG(GM-VFNS) due to the choice of pQCD scales. See text for details on the PYTHIA 8 and POWHEG event generator settings.

work [96], matched with PYTHIA 6 to generate the parton shower, and the CT14NLO parton distribution functions [97]. The nominal factorization and renormalization scales, μ_F and μ_R , were taken to be equal to the transverse mass of the quark, $\mu_0 = \sqrt{m^2 + p_T^2}$, and the charm-quark mass was set to $m_c = 1.5$ GeV/ c^2 . The theoretical uncertainties were estimated by varying these scales in the range $0.5\mu_0 < \mu_{R,F} < 2.0\mu_0$, with $0.5\mu_0 < \mu_R/\mu_F < 2.0\mu_0$. Results are also compared with recent GM-VFNS pQCD calculations [98]. With respect to previous GM-VFNS calculations [10,11], a new fragmentation function for Λ_c^+ has been used, obtained from a fit to OPAL data [99] and measurements from Belle at $\sqrt{s} = 10.52$ GeV [100]. The measured p_T -differential cross section is significantly underestimated by the POWHEG prediction, by a factor of up to 15 in the lowest p_T interval of the measurements, and around a factor 2.5 in the highest. While the discrepancy between the data and calculation decreases as the p_T increases, the measured cross section at $8 < p_T < 12$ GeV/ c is still $\sim 50\%$ larger than the upper edge of the POWHEG uncertainty band. The discrepancy between the data and POWHEG is similar to what was observed in pp collisions at $\sqrt{s} = 7$ TeV [14]. The GM-VFNS predictions also significantly underestimate the data, by about a factor of 3–4 at low p_T and by about a factor of 1.5 at high p_T .

In Fig. 6, the Λ_c^+ -production cross section in pp collisions at $\sqrt{s} = 5.02$ TeV is compared with the measurement at $\sqrt{s} = 7$ TeV [14]. For a direct comparison, the intervals $4 < p_T < 5$ GeV/ c and $5 < p_T < 6$ GeV/ c of the $\sqrt{s} = 5.02$ TeV analysis have been merged. When merging, the systematic uncertainties were propagated considering the uncertainty due to the raw-yield extraction as fully uncorrelated and all the other sources as fully correlated between p_T intervals. In the lower panel of the same figure, the ratio of the cross sections is shown. In this case, the systematic uncertainties on feed-down, p_T shape, and branching ratio were assumed to be fully correlated, while all the other sources were considered as uncorrelated between the results at the two collision energies. The relative statistical uncertainties in the measurement at $\sqrt{s} = 5.02$ TeV are on average smaller than those in the measurement at $\sqrt{s} = 7$ TeV by a factor ~ 1.5 . As expected, a lower Λ_c^+ -production cross section is observed at the lower collision energy. The difference between the cross sections at the two \sqrt{s} values increases with increasing p_T , indicating a harder p_T shape at the higher collision energy. This behavior is consistent with that observed for the D -meson cross section ratios at $\sqrt{s} = 7$ TeV and $\sqrt{s} = 5.02$ TeV, which is described by pQCD calculations [9].

Figure 7 shows the p_T -differential cross section averaged among the decay channels and analysis techniques in p -Pb

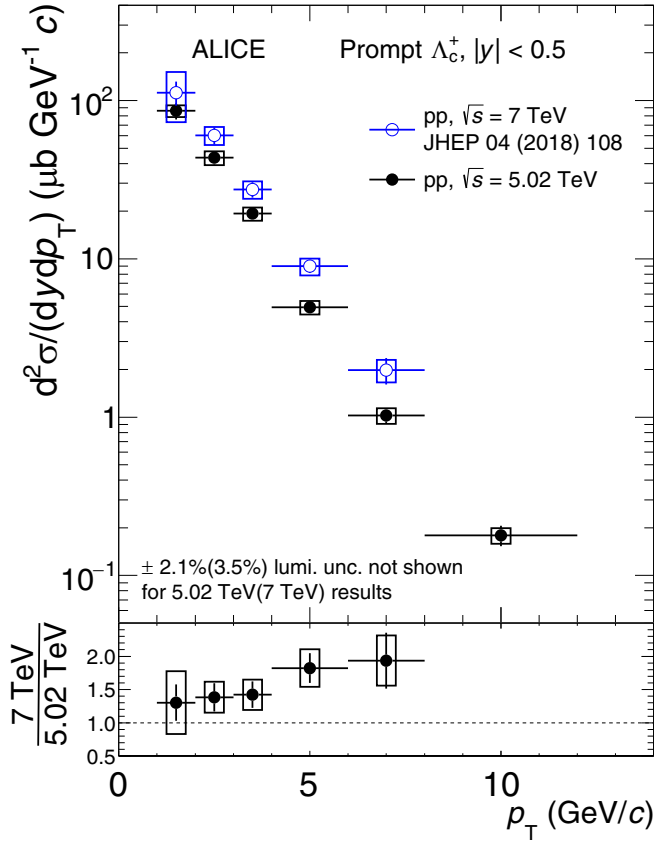


FIG. 6. Comparison between the p_T -differential production cross section of prompt Λ_c^+ baryons in pp collisions at $\sqrt{s} = 7$ TeV [14] and $\sqrt{s} = 5.02$ TeV. The ratio between the cross sections is shown in the lower panel. The statistical uncertainties are shown as vertical bars and the systematic uncertainties are shown as boxes.

collisions. The cross section is compared to the POWHEG event generator, where the generator settings, the parton shower, and the set of parton distribution functions are the same as used in the calculations for pp collisions, and the nuclear modification of the parton distribution functions is modelled with the EPPS16 nPDF parametrization [48]. The theoretical uncertainty includes the uncertainty on the factorization and renormalization scales (estimated as done for POWHEG predictions for pp collisions), while the uncertainties on the parton distribution functions and EPPS16 nPDF are not included in the calculation as they are smaller than the scale uncertainties. The cross section is underestimated by the POWHEG prediction by a factor of up to 15 in the lowest p_T intervals, similar to what is observed for pp collisions. The difference between the POWHEG predictions and the measured cross section decreases with increasing p_T and in the highest p_T interval of the measurement ($12 < p_T < 24$ GeV/c) the data point lies on the upper edge of the POWHEG uncertainty band. The Run 2 p -Pb results are compatible with our previous results from the sample of p -Pb collisions at $\sqrt{s_{NN}} = 5.02$ TeV collected in LHC Run 1 [14]. The statistical uncertainties have been reduced by approximately a factor of two for all

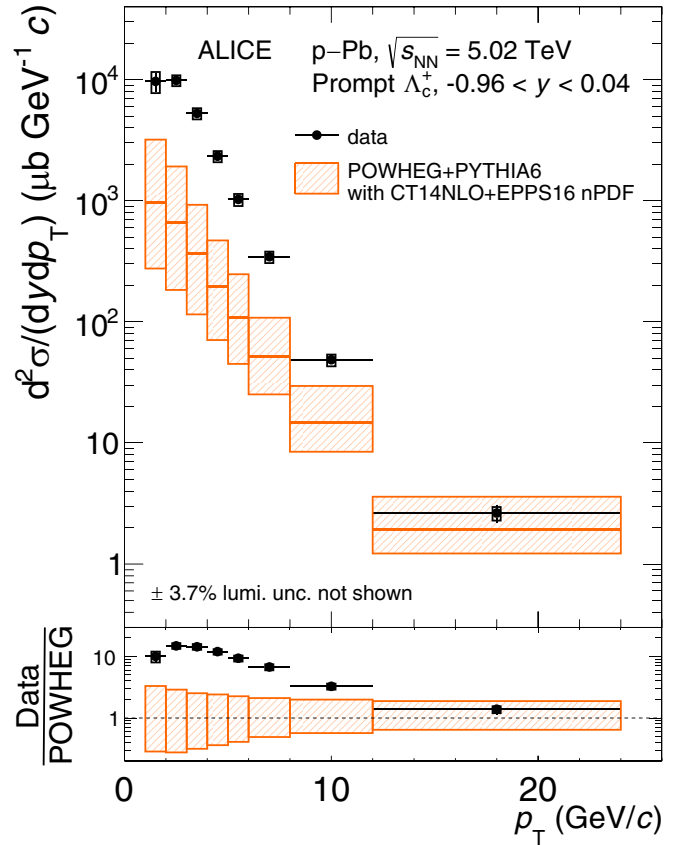


FIG. 7. p_T -differential prompt Λ_c^+ -baryon production cross section in p -Pb collisions at $\sqrt{s_{NN}} = 5.02$ TeV in the interval $1 < p_T < 24$ GeV/c compared to predictions from the POWHEG event generator [96]. The statistical uncertainties are shown as vertical bars and the systematic uncertainties are shown as boxes. The orange boxes represent the uncertainties of POWHEG due to the choice of pQCD scales. See text for details on the POWHEG event generator settings.

p_T intervals, and the systematic uncertainties improved by approximately 30% at low p_T and 10% at high p_T .

B. Nuclear modification factor

The nuclear modification factor R_{pPb} was calculated as the p_T -differential Λ_c^+ cross section in p -Pb collisions divided by the reference measurement of the p_T -differential Λ_c^+ cross section in pp collisions scaled by the lead mass number $A = 208$,

$$R_{pPb} = \frac{1}{A} \frac{d\sigma_{pPb}/dp_T}{d\sigma_{pp}/dp_T}, \quad (6)$$

where $d\sigma_{pp}/dp_T$ was obtained from the cross section measured in pp collisions in $|y| < 0.5$ applying a correction factor to account for the different rapidity coverage of the pp and p -Pb measurements. The correction factor is calculated with FONLL and ranges from 0.995 (in $1 < p_T < 2$ GeV/c) to 0.983 (in $8 < p_T < 12$ GeV/c). Figure 8 (left) shows the R_{pPb} of Λ_c^+ baryons in the p_T interval $1 < p_T < 12$ GeV/c compared to the R_{pPb} of nonstrange D mesons from Ref. [101]. With respect to the previous measurement of the Λ_c^+ -baryon

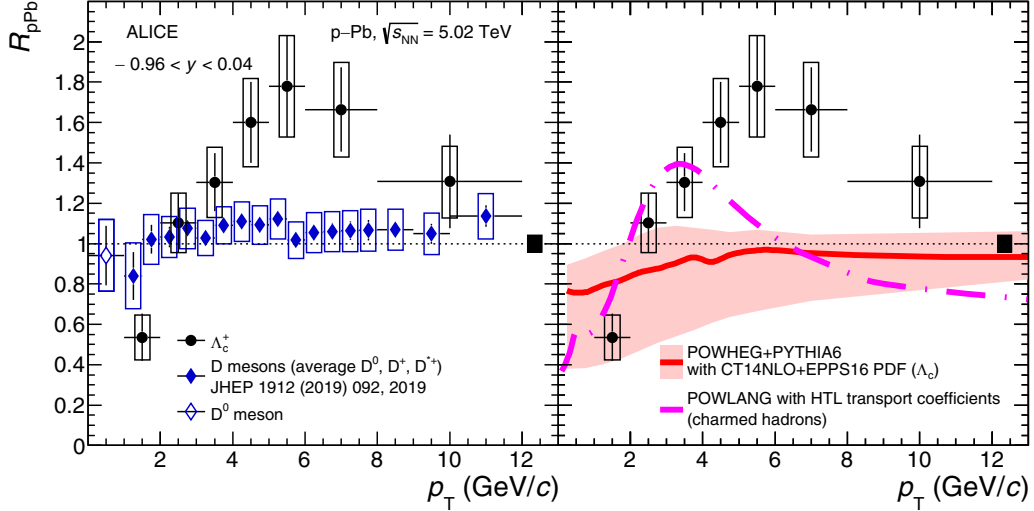


FIG. 8. The nuclear modification factor R_{pPb} of prompt Λ_c^+ baryons in p -Pb collisions at $\sqrt{s_{NN}} = 5.02$ TeV as a function of p_T , compared to the R_{pPb} of D mesons [101] (average of D^0 , D^+ , and D^{*+} in the range $1 < p_T < 12$ GeV/ c and D^0 in $0 < p_T < 1$ GeV/ c) (left), as well as to POWHEG+PYTHIA 6 [96] with EPPS16 [48] simulations, and POWLANG [60] predictions (right). The black-filled box at $R_{pPb} = 1$ represents the normalization uncertainty.

R_{pPb} [14], the p_T reach has been extended to higher and lower p_T . In addition, the pp reference at the same per-nucleon center-of-mass energy as the p -Pb sample eliminates the uncertainty originating from the \sqrt{s} -scaling of the pp cross section measured at $\sqrt{s} = 7$ TeV that was present in the previous results. These improvements, along with the increased statistical precision, have allowed for a reduction of the overall uncertainty of the R_{pPb} by a factor of 1.7–2 compared with the previous measurement. The result is consistent with the D -meson R_{pPb} within the uncertainties in the p_T regions $1 < p_T < 4$ GeV/ c and $p_T > 8$ GeV/ c , but larger than the D -meson R_{pPb} in $4 < p_T < 8$ GeV/ c with a maximum deviation of 1.9σ in $5 < p_T < 6$ GeV/ c , where σ is defined as the quadratic sum of the statistical and the lower(upper) systematic uncertainties for Λ_c^+ baryons (D mesons). For $p_T > 2$ GeV/ c the Λ_c^+ -baryon R_{pPb} is systematically above unity, with a maximum deviation from $R_{pPb} = 1$ reaching 2.2σ in the p_T interval $5 < p_T < 6$ GeV/ c , where σ is defined as the quadratic sum of the statistical and the upper systematic uncertainty. In the p_T interval $1 < p_T < 2$ GeV/ c the R_{pPb} is lower than unity by 2.6σ . This hints that Λ_c^+ production is suppressed at low p_T and is enhanced at mid- p_T in p -Pb collisions with respect to pp collisions. In Fig. 8 (right) the measured Λ_c^+ -baryon R_{pPb} is compared to model calculations. The POWHEG+PYTHIA 6 simulations use the POWHEG event generator with PYTHIA 6 parton shower and EPPS16 parametrization of the nuclear modification of the PDFs [48]. The uncertainty band includes the uncertainties on the nuclear PDFs and on the choice of the pQCD scales. The POWLANG model [60] assumes that a hot deconfined medium is formed in p -Pb collisions, and the transport of heavy quarks through an expanding QGP is computed utilising the Langevin approach and Hard Thermal Loop (HTL) transport coefficients. The POWLANG model does not implement specific differences in hadronization mechanisms for baryons and mesons, and the same prediction holds for all charm hadron species.

The two models capture some features of the data, but neither of them can quantitatively reproduce the observed Λ_c^+ -baryon R_{pPb} in the measured p_T interval.

C. p_T -integrated Λ_c^+ cross sections

The visible Λ_c^+ cross section was computed by integrating the p_T -differential cross section in its measured range. In the integration, the systematic uncertainties were propagated considering the uncertainty due to the raw-yield extraction as fully uncorrelated and all the other sources as fully correlated between p_T intervals. The visible Λ_c^+ cross section in pp collisions at $\sqrt{s} = 5.02$ TeV is

$$d\sigma_{pp, 5.02 \text{ TeV}}^{\Lambda_c^+} / dy \Big|_{|y| < 0.5}^{1 < p_T < 12 \text{ GeV}/c} = 161 \pm 11 \text{ (stat.)} \pm 14 \text{ (syst.)} \pm 3 \text{ (lumi.)} \mu\text{b}. \quad (7)$$

The visible Λ_c^+ cross section in p -Pb collisions is

$$d\sigma_{pPb, 5.02 \text{ TeV}}^{\Lambda_c^+} / dy \Big|_{-0.96 < y < 0.04}^{1 < p_T < 24 \text{ GeV}/c} = 29.0 \pm 2.0 \text{ (stat.)} \pm 3.6 \text{ (syst.)} \pm 1.1 \text{ (lumi.)} \text{ mb}. \quad (8)$$

The p_T -integrated Λ_c^+ production cross section at midrapidity was obtained by extrapolating the visible cross sections to the full p_T range. The extrapolation approach used for D mesons [75], based on the p_T -differential cross sections predicted by FONLL calculations, is not applicable here because FONLL does not have predictions for Λ_c^+ baryons. For pp collisions, PYTHIA 8 predictions with specific tunes implementing CR mechanisms were used for the extrapolation. The p_T -differential Λ_c^+ cross section values in $0 < p_T < 1$ GeV/ c and for $p_T \geq 12$ GeV/ c were obtained by scaling the measured Λ_c^+ cross section in $1 < p_T < 12$ GeV/ c for the fractions of cross section given by PYTHIA in $0 < p_T < 1$ GeV/ c and for $p_T \geq 12$ GeV/ c respectively. The PYTHIA 8 simulation with Mode 2 CR tune [24] including soft QCD processes, which gives the best description of both the magni-

tude and shape of the Λ_c^+ cross section and Λ_c^+/D^0 ratio, was used to calculate the central value of the extrapolation factors. The procedure was repeated considering the three modes defined in Ref. [24], with the envelopes of the corresponding results assigned as the extrapolation uncertainty. A second extrapolation method was also implemented as a cross-check. This consisted of multiplying the measured D^0 cross section value in $0 < p_T < 1$ GeV/c by the Λ_c^+/D^0 ratio estimated with PYTHIA 8 (CR Mode 2) in the same p_T interval to get an estimate of the Λ_c^+ cross section value in $0 < p_T < 1$ GeV/c, and then integrating in p_T . The results obtained with the two methods were found to be compatible within the uncertainties.

The resulting p_T -integrated cross section of the Λ_c^+ baryon in pp collisions at $\sqrt{s} = 5.02$ TeV is

$$d\sigma_{pp, 5.02 \text{ TeV}}^{\Lambda_c^+}/dy|_{|y|<0.5} = 230 \pm 16 \text{ (stat.)} \pm 20 \text{ (syst.)} \\ \pm 5 \text{ (lumi.)}_{-10}^{+5} \text{ (extrap.)} \mu\text{b.} \quad (9)$$

In p -Pb collisions, the p_T -integrated Λ_c^+ -production cross section was obtained using a different approach, since the p_T spectrum of Λ_c^+ is not well described by PYTHIA or other event generators. In this case, the cross sections in $0 < p_T < 1$ GeV/c and $p_T > 24$ GeV/c were calculated as the product of the pp cross sections in these p_T intervals obtained from the extrapolation of the measured p_T -differential cross section, as described above; the Pb mass number; a correction factor to account for the different rapidity interval covered in pp and p -Pb collisions; and an assumption on the nuclear modification factor R_{pPb} as described hereafter. For $0 < p_T < 1$ GeV/c, the R_{pPb} was taken as $R_{pPb} = 0.5$ as in the $1 < p_T < 2$ GeV/c interval, under the hypothesis that the trend of the Λ_c^+ R_{pPb} at low p_T is similar to that of D mesons. The uncertainty was estimated by varying the hypothesis in the range $0.35 < R_{pPb} < 0.8$, which incorporates the envelope of the available models (see Fig. 8) and the range defined by the combination of the statistical and systematic uncertainties of the Λ_c^+ R_{pPb} in $1 < p_T < 2$ GeV/c. For $p_T > 24$ GeV/c, the R_{pPb} was assumed to be equal to unity, with the range $0.8 < R_{pPb} < 1.2$ used to define the uncertainty.

The resulting p_T -integrated cross section of prompt Λ_c^+ in p -Pb collisions at $\sqrt{s_{NN}} = 5.02$ TeV is

$$d\sigma_{pPb, 5.02 \text{ TeV}}^{\Lambda_c^+}/dy|_{-0.96 < y < 0.04} \\ = 36.2 \pm 2.5 \text{ (stat.)} \pm 4.5 \text{ (syst.)} \\ \pm 1.3 \text{ (lumi.)}_{-2.7}^{+4.4} \text{ (extrap.)} \text{ mb.} \quad (10)$$

The visible cross sections make up 70% and 80% of the integrated cross sections in pp and p -Pb collisions, respectively. The p_T -integrated Λ_c^+ cross sections in pp and p -Pb collisions can be used for the comparison of fragmentation fractions of charm quarks in different collision systems and rapidity intervals. They can also be used in the calculation of the $c\bar{c}$ cross section together with the cross sections of D mesons and higher-mass charm baryons that do not decay into Λ_c^+ . Due to the lack of measurements of higher-mass charm baryons ($\Xi_c^{+,0}, \Omega_c$) at $\sqrt{s} = 5.02$ TeV, which contribute to the $c\bar{c}$ cross section, a calculation of the $c\bar{c}$ cross section is beyond the scope of this work.

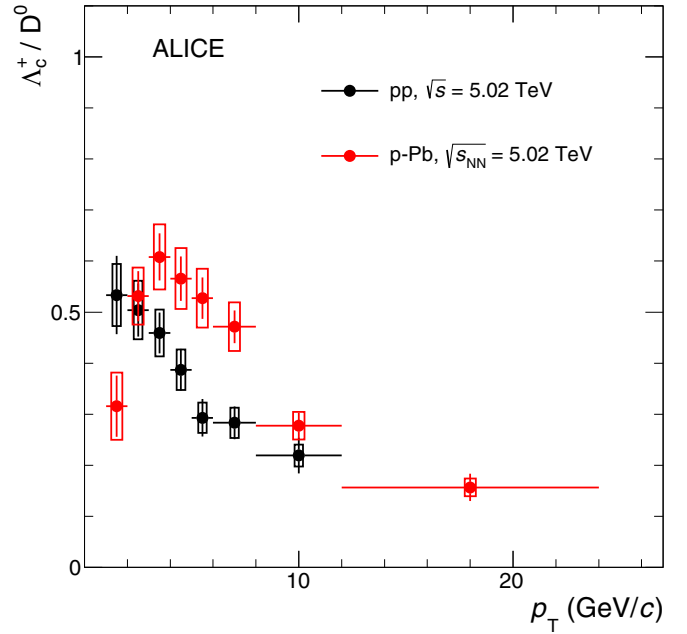


FIG. 9. The Λ_c^+/D^0 ratio as a function of p_T measured in pp collisions at $\sqrt{s} = 5.02$ TeV and in p -Pb collisions at $\sqrt{s_{NN}} = 5.02$ TeV.

D. Λ_c^+/D^0 ratios

The ratios between the yields of Λ_c^+ baryons and D^0 mesons were calculated using the D^0 cross sections reported in Ref. [9] for pp collisions and [101] for p -Pb collisions, respectively. The uncertainty sources assumed to be uncorrelated between the Λ_c^+ and D^0 production cross sections include those due to the raw-yield extraction, the selection efficiency, the PID efficiency, the generated p_T shape, the $(A \times \epsilon)$ statistical uncertainties, and the branching ratios. The uncertainties assumed to be correlated include those due to the tracking, the beauty feed-down and the luminosity. The D^0 cross section was measured in finer p_T intervals than the Λ_c^+ , so it was rebinned such that the p_T intervals match between the two species.

The Λ_c^+/D^0 ratio as a function of p_T in pp and p -Pb collisions is shown in Fig. 9. A clear decreasing trend with increasing p_T is seen in both pp and p -Pb collisions for $p_T > 2$ GeV/c, and at high p_T the ratio reaches a value of about 0.2. The ratios measured in pp and p -Pb collisions are qualitatively consistent with each other, although a larger Λ_c^+/D^0 ratio in $3 < p_T < 8$ GeV/c and a lower ratio in $1 < p_T < 2$ GeV/c are measured in p -Pb collisions with respect to pp collisions.

The values of the p_T -integrated Λ_c^+/D^0 ratios are reported in Table III along with the values measured in e^+e^- and e^-p collisions by other experiments. The Λ_c^+/D^0 ratios in pp and p -Pb collisions are consistent with each other within the experimental uncertainties. Comparing to previous measurements in other collision systems, the Λ_c^+/D^0 ratio is significantly enhanced by a factor of about 3–5 in pp collisions and a factor of about 2–4 in p -Pb collisions, indicating that the fragmentation fractions of charm quarks into baryons

TABLE III. Comparison of the p_T -integrated Λ_c^+/D^0 ratio measured in pp and p -Pb collisions and the same ratios in e^+e^- and e^-p collisions (reproduced from Ref. [14]). Statistical and systematic uncertainties are reported (from Refs. [15,17] it was not possible to separate systematics and statistical uncertainties). The ALICE measurements report an additional uncertainty source from the extrapolation procedure.

	$\Lambda_c^+/D^0 \pm \text{stat.} \pm \text{syst.}$	System	\sqrt{s} (GeV)	Notes
ALICE	$0.51 \pm 0.04 \pm 0.04^{+0.01}_{-0.02}$	pp	5020	$p_T > 0, y < 0.5$ $p_T > 0, -0.96 < y < 0.04$
ALICE	$0.42 \pm 0.03 \pm 0.06^{+0.05}_{-0.03}$	p -Pb	5020	
CLEO [16]	$0.119 \pm 0.021 \pm 0.019$	e^+e^-	10.55	$1 < Q^2 < 1000 \text{ GeV}^2,$ $0 < p_T < 10 \text{ GeV}/c, 0.02 < y < 0.7,$ $130 < W < 300 \text{ GeV}, Q^2 < 1 \text{ GeV}^2,$ $p_T > 3.8 \text{ GeV}/c, \eta < 1.6$ $130 < W < 300 \text{ GeV}, Q^2 < 1 \text{ GeV}^2,$ $p_T > 3.8 \text{ GeV}/c, \eta < 1.6$
ARGUS [15,17]	0.127 ± 0.031	e^+e^-	10.55	
LEP average [18]	$0.113 \pm 0.013 \pm 0.006$	e^+e^-	91.2	
ZEUS DIS [21]	$0.124 \pm 0.034^{+0.025}_{-0.022}$	e^-p	320	
ZEUS $\gamma p,$	$0.220 \pm 0.035^{+0.027}_{-0.037}$	e^-p	320	
HERA I [19]				
ZEUS $\gamma p,$	$0.107 \pm 0.018^{+0.009}_{-0.014}$	e^-p	320	
HERA II [20]				

are different with respect to e^+e^- and e^-p collisions. This is consistent with the previous ALICE measurements [14], where the p_T -integrated Λ_c^+/D^0 ratios were restricted to $1 < p_T < 8 \text{ GeV}/c$ in pp collisions, and to $2 < p_T < 12 \text{ GeV}/c$ in p -Pb collisions.

Figure 10 shows the Λ_c^+/D^0 ratio in pp collisions compared with models from MC generators, and a statistical hadronization model. The MC generators include PYTHIA 8 with Monash tune and color reconnection tunes as described above; PYTHIA 8 with color reconnection plus rope hadronization [24,102] where color charges can act coherently to form a rope, increasing the effective string tension; HERWIG 7.2 [27] where hadronization is implemented via clusters; and POWHEG pQCD generator matched to PYTHIA

6 to generate the parton shower, as described above. The measured points are also compared to predictions from GM-VFNS pQCD calculations, which were computed as the ratios of the Λ_c^+ and D^0 cross sections obtained with the same choice of pQCD scales [98]. The left panel shows the predictions of the Λ_c^+/D^0 ratio from PYTHIA 8 (Monash tune), HERWIG 7, POWHEG, and GM-VFNS, which all implement fragmentation processes tuned on charm production measurements in e^+e^- collisions, and therefore all predict a value of the Λ_c^+/D^0 ratio around 0.1, with a very mild p_T dependence. These predictions significantly underestimate the data at low p_T by a factor of about 5–10, while at high p_T the discrepancy is reduced to a factor of about 2. The right panel shows models which include processes that enhance baryon

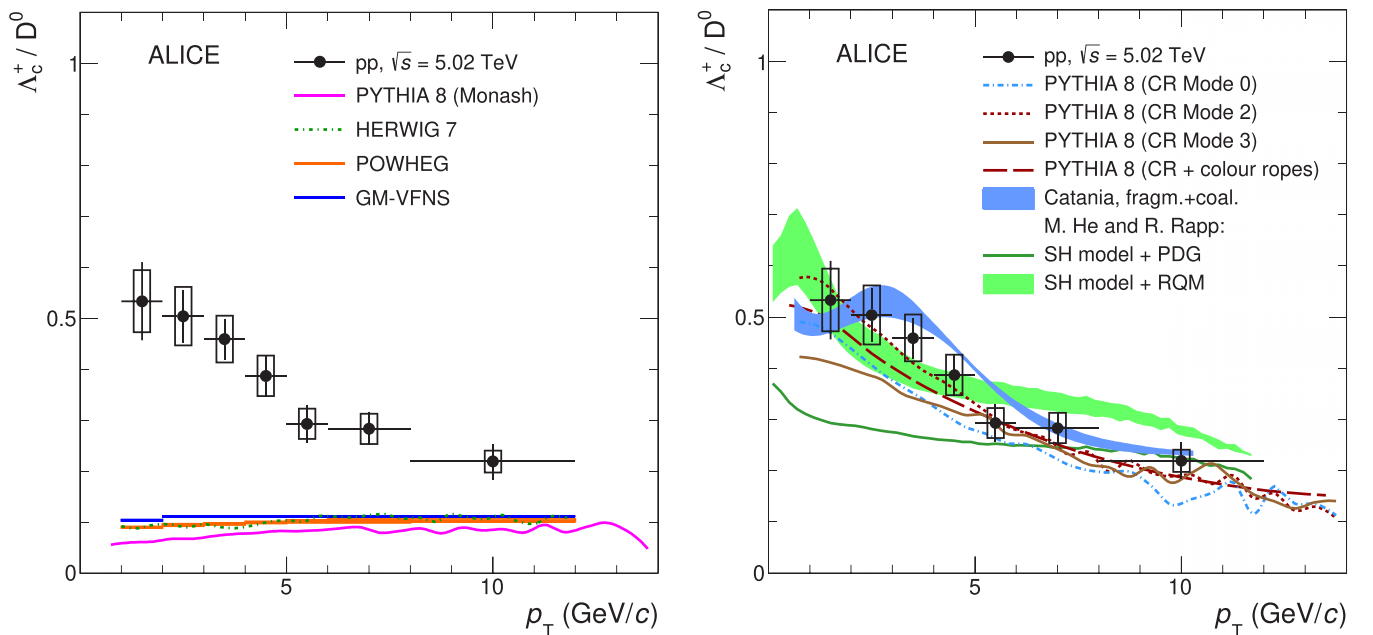


FIG. 10. The Λ_c^+/D^0 ratio measured in pp collisions at $\sqrt{s} = 5.02 \text{ TeV}$, compared to theoretical predictions. The measurement is compared with predictions from MC generators (PYTHIA 8 [23,24], HERWIG 7 [27], POWHEG [96]), GM-VFNS [98], a statistical hadronization model [72] (“SH model” in the legend) and a model which implements hadronization via coalescence and fragmentation [104]. See text for model details.

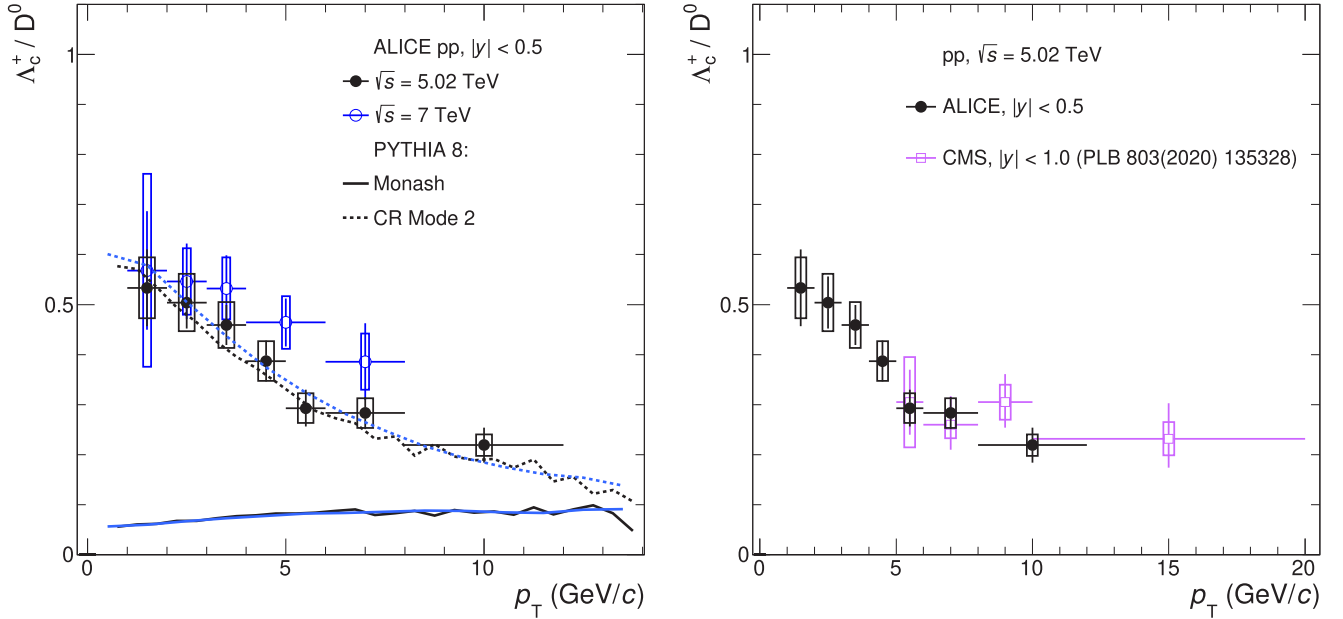


FIG. 11. Left: The Λ_c^+/D^0 ratio measured in pp collisions at $\sqrt{s} = 5.02$ TeV, compared to the measurement at $\sqrt{s} = 7$ TeV [14]. PYTHIA 8 predictions are shown at both energies, for the Monash tune (solid lines) and with the Mode 2 CR tune (dotted lines). Right: the Λ_c^+/D^0 ratio at $\sqrt{s} = 5.02$ TeV compared with the measurement by the CMS Collaboration at $|y| < 1$ [28].

production. A significant enhancement of the Λ_c^+/D^0 ratio is observed with PYTHIA 8 simulations including CR beyond the leading-color approximation, with respect to the Monash tune. The results of these PYTHIA 8 tunes are consistent with the measured Λ_c^+/D^0 ratio in pp collisions, also reproducing the decreasing trend of Λ_c^+/D^0 with increasing p_T . Including rope hadronization in addition to color reconnection induces a small modification in the Λ_c^+/D^0 ratio, suggesting that the increased string tension does not significantly affect the relative production of baryons with respect to mesons. The data is also compared with a statistical hadronization model [72] where the underlying charm baryon spectrum is either taken from the PDG, or augmented to include additional excited baryon states, which have not yet been observed but are predicted by the Relativistic Quark Model (RQM) [103]. For the former case, the model underpredicts the data at low p_T . For the latter case, the additional charm baryon states decay strongly to Λ_c^+ baryons, contributing to the prompt Λ_c^+ spectrum. This increases the Λ_c^+/D^0 ratio and allows the model to describe both the magnitude and the p_T dependence of the measured ratio. Finally, the Catania model [104] is also presented, which assumes that a QGP is formed in pp collisions and that the hadronization occurs via coalescence as well as fragmentation. The light quark p_T spectrum is determined with a blast wave model, while the heavy quark p_T spectrum is determined with FONLL pQCD predictions, and coalescence is implemented via the Wigner formalism. Contrary to the implementation in Pb–Pb collisions [105], jet quenching mechanisms are not included in pp collisions. The model predicts that hadronization via coalescence is dominant at low p_T , while fragmentation dominates at high p_T . Both the magnitude and the p_T shape of the measured Λ_c^+/D^0 ratio are described well by this model.

Figure 11 (left) shows the Λ_c^+/D^0 ratio in pp collisions at $\sqrt{s} = 5.02$ TeV compared with the previous measurement at $\sqrt{s} = 7$ TeV, and with predictions from PYTHIA 8 simulations. The Λ_c^+/D^0 ratio is found to be consistent between the two collision energies, within the experimental uncertainties; however, the wider p_T coverage and the improved statistical and systematic uncertainties on the new measurement reveal a clear decreasing trend in the Λ_c^+/D^0 ratio in pp collisions at $\sqrt{s} = 5.02$ TeV, which was not clearly visible in the result at $\sqrt{s} = 7$ TeV. The predictions of PYTHIA 8 with Monash tune do not show a \sqrt{s} -dependence, while those with CR Mode 2 indicate a slight \sqrt{s} -dependence, where the Λ_c^+/D^0 ratio is slightly larger at low p_T at $\sqrt{s} = 7$ TeV than at $\sqrt{s} = 5.02$ TeV. The right panel shows the Λ_c^+/D^0 ratio in pp collisions, compared with the measurement by the CMS Collaboration in $5 < p_T < 20$ GeV/c and $|y| < 1$ [28]. In the p_T region covered by both experiments, the results are found to be consistent with one another.

In Fig. 12, the Λ_c^+/D^0 ratio in p –Pb collisions at midrapidity ($-0.96 < y < 0.04$) is compared with the measurements by the LHCb Collaboration at forward ($1.5 < y < 4$) and backward ($-4.5 < y < -2.5$) rapidities [71]. The left panel shows the comparison of the Λ_c^+/D^0 ratios in the different rapidity intervals as a function of p_T . For $p_T < 8$ GeV/c the ratio measured at midrapidity is higher than the ones measured at forward and backward rapidities, whereas at higher p_T the measurements are consistent within uncertainties. The right panel shows the p_T -integrated Λ_c^+/D^0 ratio as a function of rapidity. The p_T range of the integration of the ALICE data ($2 < p_T < 12$ GeV/c) is chosen to be similar to the reported LHCb integrated p_T range ($2 < p_T < 10$ GeV/c). The results suggest an enhancement of the ratio at midrapidity with respect to forward and backward rapidities. The difference between the Λ_c^+/D^0 ratio at mid and forward (backward)

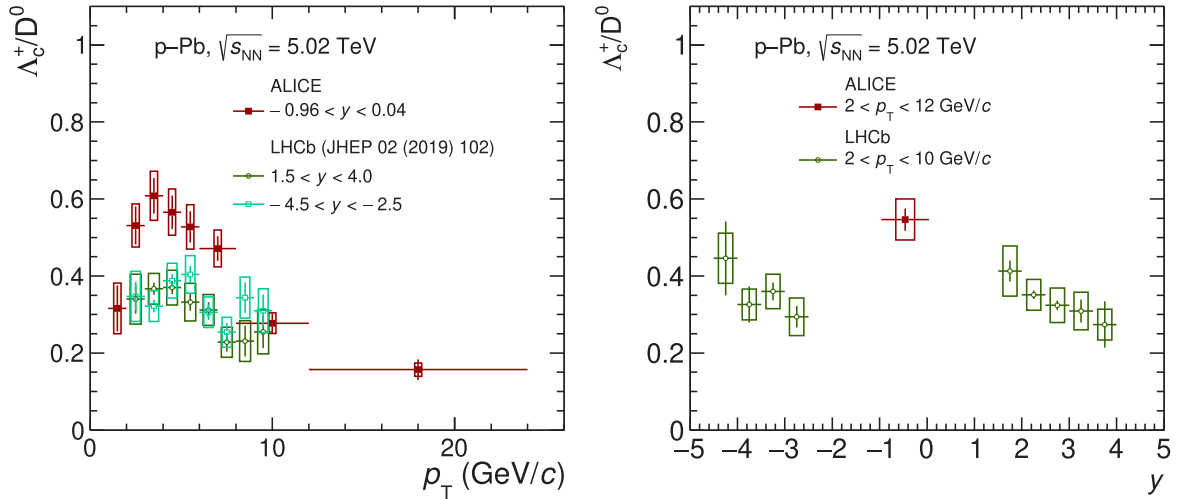


FIG. 12. The Λ_c^+/D^0 ratio measured in p -Pb collisions at $\sqrt{s_{NN}} = 5.02$ TeV, compared with the measurement at forward and backward rapidity [71] by the LHCb collaboration. The measurements are shown as a function of p_T (left) and as a function of y (right).

rapidities is less pronounced in p -Pb collisions compared to the one observed in pp collisions at 7 TeV [14,29].

Figure 13 shows the Λ_c^+/D^0 ratio in pp and p -Pb collisions, compared to the baryon-to-meson ratios in the light-flavor sector, p/π [68,106] and Λ/K_S^0 [107,108]. The p/π ratio in pp collisions is shown at center-of-mass energies of 7 TeV and 5.02 TeV, and both results are fully consistent with each other. The Λ/K_S^0 ratio in pp collisions is shown at $\sqrt{s} = 7$ TeV. Comparing the Λ_c^+/D^0 ratio to the light-flavor ratios, similar characteristics can be seen. All the baryon-to-meson ratios decrease with increasing p_T for $p_T > 3$ GeV/c. In addition, the light-flavor hadron ratios show a distinct peak at intermediate p_T (around 3 GeV/c), while the Λ_c^+/D^0 ratio shows a hint of a peak at $2 < p_T < 4$ GeV/c in p -Pb

collisions, though a higher precision measurement would be needed to confirm this. Also shown in Fig. 13 are predictions from PYTHIA 8 with Monash and CR Mode 2 tunes. The PYTHIA 8 predictions for the light-flavor baryon-to-meson ratios are calculated at $\sqrt{s} = 7$ TeV. It can be observed that the behaviors of the PYTHIA 8 predictions for light-flavor and charm baryon-to-meson ratios are similar. The measured Λ/K_S^0 ratio in pp collisions is underestimated by the Monash tune, while for the CR Mode 2 tune both the magnitude and trend of the ratio are closer to data, despite predicting a slightly flatter trend with p_T . The p/π ratio is underestimated by PYTHIA 8 (Monash) at low p_T but overestimated at high p_T , while CR Mode 2 improves the agreement with data at low p_T but still overestimates the data at high p_T . Overall, the

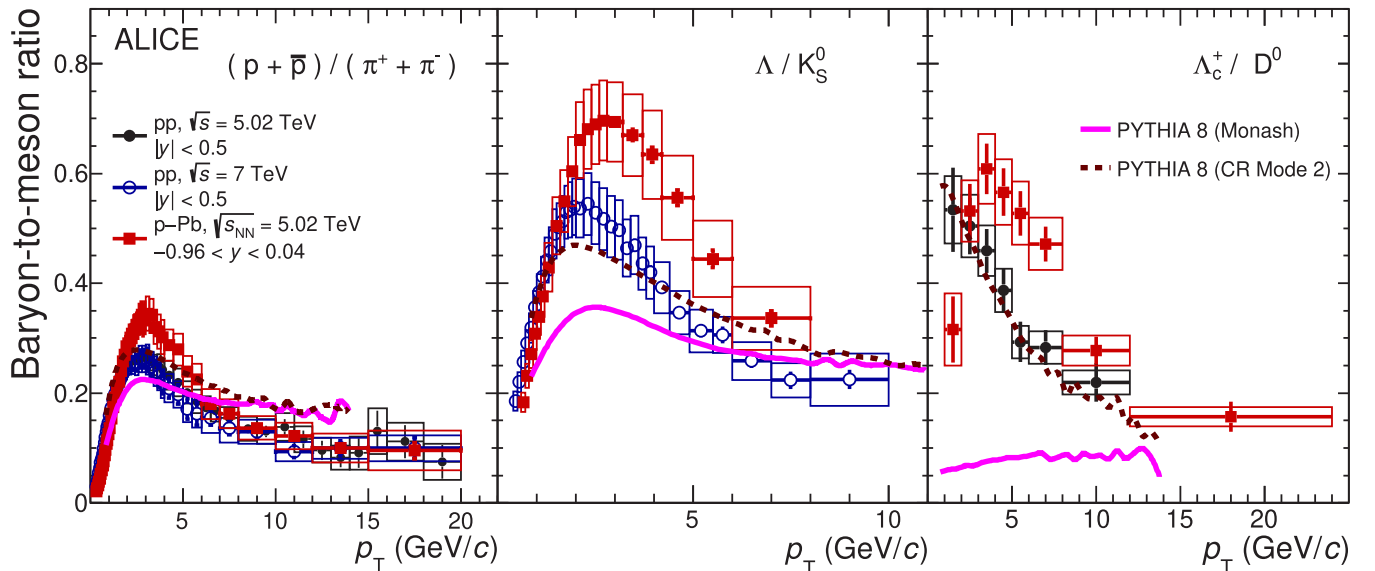


FIG. 13. The baryon-to-meson ratios in the light-flavor and charm sector; p/π in pp collisions at $\sqrt{s} = 5.02$ TeV and 7 TeV and p -Pb collisions at $\sqrt{s_{NN}} = 5.02$ TeV [68] (left), Λ/K_S^0 in pp collisions at $\sqrt{s} = 7$ TeV and p -Pb collisions at $\sqrt{s_{NN}} = 5.02$ TeV [107,108] (middle), and Λ_c^+/D^0 in pp collisions at $\sqrt{s} = 5.02$ TeV and p -Pb collisions at $\sqrt{s_{NN}} = 5.02$ TeV (right). The data are compared to predictions from PYTHIA 8 [23,24]. See text for model details.

color reconnection modes in PYTHIA 8 generally provide a better description of the baryon-to-meson ratios in both the light-flavor and charm sector.

VII. SUMMARY AND CONCLUSIONS

The measurements of the production of prompt Λ_c^+ baryons at midrapidity in pp collisions at $\sqrt{s} = 5.02$ TeV and in p -Pb collisions at $\sqrt{s_{NN}} = 5.02$ TeV with the ALICE detector at the LHC have been reported. The measurement in pp collisions, in particular, was performed at a different center-of-mass energy with respect to the previous work in which Λ_c^+ -baryon production was measured in pp collisions at $\sqrt{s} = 7$ TeV [14]. The pp data sample at $\sqrt{s} = 5.02$ TeV is the natural reference for measurements in p -Pb and Pb-Pb collisions at the same center-of-mass energy per nucleon pair. Moreover, with respect to Ref. [14], the uncertainties were significantly reduced, and the p_T range and the p_T granularity of the measurements were improved in both collision systems. The analysis was performed using two different decay channels, $\Lambda_c^+ \rightarrow pK^-\pi^+$ and $\Lambda_c^+ \rightarrow pK_S^0$. The results were reported for pp collisions in the rapidity interval $|y| < 0.5$ and the transverse-momentum interval $1 < p_T < 12$ GeV/ c and for p -Pb collisions in $-0.96 < y < 0.04$ and $1 < p_T < 24$ GeV/ c . The p_T -differential production cross sections were obtained averaging the results from different hadronic decay channels.

The p_T -differential cross section was measured to be larger than predictions given by pQCD calculations in both pp and p -Pb collisions. The nuclear modification factor R_{pPb} of Λ_c^+ baryons was found to be below unity in the interval $1 < p_T < 2$ GeV/ c and to peak above unity around 5 GeV/ c . It is consistent with the R_{pPb} of D mesons in the p_T regions $1 < p_T < 4$ GeV/ c and $p_T > 8$ GeV/ c and larger than the D -meson R_{pPb} in $4 < p_T < 8$ GeV/ c . The current precision of the measurement is not enough to draw conclusions on the role of different CNM effects and the possible presence of hot-medium effects. As already observed in Ref. [14], the Λ_c^+/D^0 baryon-to-meson ratio in pp collisions is larger than previous measurements obtained in e^+e^- and e^-p collision systems at lower center-of-mass energies. The increase of precision in this paper allowed to observe, for the first time, a clear decreasing trend as a function of transverse momentum in the Λ_c^+/D^0 ratio. The Λ_c^+/D^0 ratio was compared to pp event generators and models that implement different particle production and hadronization mechanisms: qualitative agreement with the measurement is obtained with PYTHIA 8 tunes including string formation beyond the leading-color approximation; a prediction based on the statistical hadronization model which includes unobserved charm baryon states that strongly decay to Λ_c^+ ; and a prediction which assumes the formation of a QGP and implements hadronization via coalescence and fragmentation. The Λ_c^+/D^0 ratio measured in pp collisions is consistent with the results by CMS at midrapidity in the common p_T regions of both measurements. The ratio in p -Pb collisions at midrapidity is higher than the one measured by LHCb at forward and backward rapidities in $2 < p_T < 8$ GeV/ c , while for $p_T > 8$ GeV/ c the measurements at central, forward and backward rapidities are

consistent within uncertainties. The measured Λ_c^+/D^0 ratio was also compared with baryon-to-meson ratios measured in the light-flavor sector. The measured Λ/K_S^0 ratio can also be described by PYTHIA 8 when including string formation beyond the leading-color approximation, although this PYTHIA 8 tune slightly overestimates the measured p/π ratio. The increased precision of this measurement with respect to the measurements made with the Run 1 data is crucial for providing further insight into charm baryon production in pp and p -Pb collisions. A more precise measurement is expected to be obtained during the LHC Runs 3 and 4 after the upgrade of the ALICE apparatus [109].

ACKNOWLEDGMENTS

The ALICE Collaboration thanks all its engineers and technicians for their invaluable contributions to the construction of the experiment and the CERN accelerator teams for the outstanding performance of the LHC complex. The ALICE Collaboration gratefully acknowledges the resources and support provided by all Grid centers and the Worldwide LHC Computing Grid (WLCG) collaboration. The ALICE Collaboration acknowledges the following funding agencies for their support in building and running the ALICE detector: A. I. Alikhanyan National Science Laboratory (Yerevan Physics Institute) Foundation (ANSL), State Committee of Science and World Federation of Scientists (WFS), Armenia; Austrian Academy of Sciences, Austrian Science Fund (FWF): [M 2467-N36] and Nationalstiftung für Forschung, Technologie und Entwicklung, Austria; Ministry of Communications and High Technologies, National Nuclear Research Center, Azerbaijan; Conselho Nacional de Desenvolvimento Científico e Tecnológico (CNPq), Financiadora de Estudos e Projetos (Finep), Fundação de Amparo à Pesquisa do Estado de São Paulo (FAPESP) and Universidade Federal do Rio Grande do Sul (UFRGS), Brazil; Ministry of Education of China (MOEC), Ministry of Science & Technology of China (MSTC) and National Natural Science Foundation of China (NSFC), China; Ministry of Science and Education and Croatian Science Foundation, Croatia; Centro de Aplicaciones Tecnológicas y Desarrollo Nuclear (CEADEN), Cubaenergía, Cuba; Ministry of Education, Youth and Sports of the Czech Republic, Czech Republic; The Danish Council for Independent Research | Natural Sciences, the VILLUM FONDEN and Danish National Research Foundation (DNRF), Denmark; Helsinki Institute of Physics (HIP), Finland; Commissariat à l'Energie Atomique (CEA) and Institut National de Physique Nucléaire et de Physique des Particules (IN2P3) and Centre National de la Recherche Scientifique (CNRS), France; Bundesministerium für Bildung und Forschung (BMBF) and GSI Helmholtzzentrum für Schwerionenforschung GmbH, Germany; General Secretariat for Research and Technology, Ministry of Education, Research and Religions, Greece; National Research, Development and Innovation Office, Hungary; Department of Atomic Energy Government of India (DAE), Department of Science and Technology, Government of India (DST), University Grants Commission, Government of India (UGC) and Council of Scientific and Industrial Research (CSIR), India; Indonesian Institute of Science, Indonesia;

Istituto Nazionale di Fisica Nucleare (INFN), Italy; Institute for Innovative Science and Technology, Nagasaki Institute of Applied Science (IIST), Japanese Ministry of Education, Culture, Sports, Science and Technology (MEXT) and Japan Society for the Promotion of Science (JSPS) KAKENHI, Japan; Consejo Nacional de Ciencia (CONACYT) y Tecnología, through Fondo de Cooperación Internacional en Ciencia y Tecnología (FONCICYT) and Dirección General de Asuntos del Personal Académico (DGAPA), Mexico; Nederlandse Organisatie voor Wetenschappelijk Onderzoek (NWO), Netherlands; The Research Council of Norway, Norway; Commission on Science and Technology for Sustainable Development in the South (COMSATS), Pakistan; Pontificia Universidad Católica del Perú, Peru; Ministry of Science and Higher Education, National Science Centre and WUT ID-UB, Poland; Korea Institute of Science and Technology Information and National Research Foundation of Korea (NRF), Republic of Korea; Ministry of Education and Scientific Research, Institute of Atomic Physics and Ministry of Research and Innova-

tion and Institute of Atomic Physics, Romania; Joint Institute for Nuclear Research (JINR), Ministry of Education and Science of the Russian Federation, National Research Centre Kurchatov Institute, Russian Science Foundation and Russian Foundation for Basic Research, Russia; Ministry of Education, Science, Research and Sport of the Slovak Republic, Slovakia; National Research Foundation of South Africa, South Africa; Swedish Research Council (VR) and Knut & Alice Wallenberg Foundation (KAW), Sweden; European Organization for Nuclear Research, Switzerland; Suranaree University of Technology (SUT), National Science and Technology Development Agency (NSDTA) and Office of the Higher Education Commission under NRU project of Thailand, Thailand; Turkish Atomic Energy Agency (TAEK), Turkey; National Academy of Sciences of Ukraine, Ukraine; Science and Technology Facilities Council (STFC), United Kingdom; National Science Foundation of the United States of America (NSF) and United States Department of Energy, Office of Nuclear Physics (DOE NP), United States of America.

-
- [1] L. Adamczyk *et al.* (STAR Collaboration), Measurements of D^0 and D^* Production in $p + p$ Collisions at $\sqrt{s} = 200$ GeV, *Phys. Rev. D* **86**, 072013 (2012).
- [2] D. Acosta *et al.* (CDF Collaboration), Measurement of Prompt Charm Meson Production Cross Sections in $p\bar{p}$ Collisions at $\sqrt{s} = 1.96$ TeV, *Phys. Rev. Lett.* **91**, 241804 (2003).
- [3] D. Acosta *et al.* (CDF Collaboration), Measurement of the J/ψ meson and b -hadron production cross sections in $p\bar{p}$ collisions at $\sqrt{s} = 1960$ GeV, *Phys. Rev. D* **71**, 032001 (2005).
- [4] A. Abulencia *et al.* (CDF Collaboration), Measurement of the B^+ production cross-section in p anti- p collisions at $s^{*1/2} = 1960$ -GeV, *Phys. Rev. D* **75**, 012010 (2007).
- [5] A. Andronic *et al.*, Heavy-flavor and quarkonium production in the LHC era: From proton-proton to heavy-ion collisions, *Eur. Phys. J. C* **76**, 107 (2016).
- [6] R. Aaij *et al.* (LHCb Collaboration), Measurements of prompt charm production cross-sections in pp collisions at $\sqrt{s} = 13$ TeV, *J. High Energy Phys.* **03** (2016) 159; **09** (2016) 013.
- [7] V. Khachatryan *et al.* (CMS Collaboration), Measurement of the total and differential inclusive B^+ hadron cross sections in pp collisions at $\sqrt{s} = 13$ TeV, *Phys. Lett. B* **771**, 435 (2017).
- [8] R. Aaij *et al.* (LHCb Collaboration), Measurement of the B^\pm production cross-section in pp collisions at $\sqrt{s} = 7$ and 13 TeV, *J. High Energy Phys.* **12** (2017) 026.
- [9] S. Acharya *et al.* (ALICE Collaboration), Measurement of D^0 , D^+ , D^{*+} , and D_s^+ production in pp collisions at $\sqrt{s} = 5.02$ TeV with ALICE, *Eur. Phys. J. C* **79**, 388 (2019).
- [10] B. A. Kniehl, G. Kramer, I. Schienbein, and H. Spiesberger, Collinear subtractions in hadroproduction of heavy quarks, *Eur. Phys. J. C* **41**, 199 (2005).
- [11] B. A. Kniehl, G. Kramer, I. Schienbein, and H. Spiesberger, Inclusive charmed-meson production at the CERN LHC, *Eur. Phys. J. C* **72**, 2082 (2012).
- [12] M. Cacciari, M. Greco, and P. Nason, The p_T spectrum in heavy-flavor hadroproduction, *J. High Energy Phys.* **05** (1998) 007.
- [13] M. Cacciari *et al.*, Theoretical predictions for charm and bottom production at the LHC, *J. High Energy Phys.* **10** (2012) 137.
- [14] S. Acharya *et al.* (ALICE Collaboration), Λ_c^+ production in pp collisions at $\sqrt{s} = 7$ TeV and in p -Pb collisions at $\sqrt{s_{NN}} = 5.02$ TeV, *J. High Energy Phys.* **04** (2018) 108.
- [15] H. Albrecht *et al.* (ARGUS Collaboration), Observation of the charmed baryon Λ_c in e^+e^- annihilation at 10-GeV, *Phys. Lett. B* **207**, 109 (1988).
- [16] P. Avery *et al.* (CLEO Collaboration), Inclusive production of the charmed baryon Λ_c from e^+e^- annihilations at $\sqrt{s} = 10.55$ GeV, *Phys. Rev. D* **43**, 3599 (1991).
- [17] H. Albrecht *et al.* (ARGUS Collaboration), Inclusive production of D^0 , D^+ and $D^*(2010)^+$ mesons in B decays and nonresonant e^+e^- annihilation at 10.6 GeV, *Z. Phys. C* **52**, 353 (1991).
- [18] L. Gladilin, Fragmentation fractions of c and b quarks into charmed hadrons at LEP, *Eur. Phys. J. C* **75**, 19 (2015).
- [19] S. Chekanov *et al.* (ZEUS Collaboration), Measurement of charm fragmentation ratios and fractions in photoproduction at HERA, *Eur. Phys. J. C* **44**, 351 (2005).
- [20] H. Abramowicz *et al.* (ZEUS Collaboration), Measurement of charm fragmentation fractions in photoproduction at HERA, *J. High Energy Phys.* **09** (2013) 058.
- [21] H. Abramowicz *et al.* (ZEUS Collaboration), Measurement of D^+ and Λ_c^+ production in deep inelastic scattering at HERA, *J. High Energy Phys.* **11** (2010) 009.
- [22] M. Lisovskyi, A. Verbytskyi, and O. Zenaiev, Combined analysis of charm-quark fragmentation-fraction measurements, *Eur. Phys. J. C* **76**, 397 (2016).
- [23] P. Skands, S. Carrazza, and J. Rojo, Tuning PYTHIA 8.1: The Monash 2013 Tune, *Eur. Phys. J. C* **74**, 3024 (2014).
- [24] J. R. Christiansen and P. Z. Skands, String formation beyond leading color, *J. High Energy Phys.* **08** (2015) 003.

- [25] C. Bierlich and J. R. Christiansen, Effects of color reconnection on hadron flavor observables, *Phys. Rev. D* **92**, 094010 (2015).
- [26] C. Flensburg, G. Gustafson, and L. Lonnblad, Inclusive and exclusive observables from dipoles in high energy collisions, *J. High Energy Phys.* **08** (2011) 103.
- [27] J. Bellm *et al.*, Herwig 7.0/Herwig++ 3.0 release note, *Eur. Phys. J. C* **76**, 196 (2016).
- [28] A. M. Sirunyan *et al.* (CMS Collaboration), Production of Λ_c^+ baryons in proton-proton and lead-lead collisions at $\sqrt{s_{NN}} = 5.02$ TeV, *Phys. Lett. B* **803**, 135328 (2020).
- [29] R. Aaij *et al.* (LHCb Collaboration), Prompt charm production in pp collisions at $\sqrt{s} = 7$ TeV, *Nucl. Phys. B* **871**, 1 (2013).
- [30] R. Maciula and A. Szczurek, Production of Λ_c baryons at the LHC within the k_T -factorization approach and independent parton fragmentation picture, *Phys. Rev. D* **98**, 014016 (2018).
- [31] R. Aaij *et al.* (LHCb Collaboration), Measurement of b -hadron production fractions in 7 TeV pp collisions, *Phys. Rev. D* **85**, 032008 (2012).
- [32] R. Aaij *et al.* (LHCb Collaboration), Study of the production of Λ_b^0 and \bar{B}^0 hadrons in pp collisions and first measurement of the $\Lambda_b^0 \rightarrow J/\psi p K^-$ branching fraction, *Chin. Phys. C* **40**, 011001 (2016).
- [33] R. Aaij *et al.* (LHCb Collaboration), Measurement of b hadron fractions in 13 TeV pp collisions, *Phys. Rev. D* **100**, 031102 (2019).
- [34] S. Chatrchyan *et al.* (CMS Collaboration), Measurement of the Λ_b cross section and the $\bar{\Lambda}_b$ to Λ_b ratio with $J/\Psi\Lambda$ decays in pp collisions at $\sqrt{s} = 7$ TeV, *Phys. Lett. B* **714**, 136 (2012).
- [35] J. Adams *et al.* (STAR Collaboration), Experimental and theoretical challenges in the search for the quark gluon plasma: The STAR Collaboration's critical assessment of the evidence from RHIC collisions, *Nucl. Phys. A* **757**, 102 (2005).
- [36] K. Adcox *et al.* (PHENIX Collaboration), Formation of dense partonic matter in relativistic nucleus-nucleus collisions at RHIC: Experimental evaluation by the PHENIX collaboration, *Nucl. Phys. A* **757**, 184 (2005).
- [37] I. Arsene *et al.* (BRAHMS Collaboration), Quark gluon plasma and color glass condensate at RHIC? The Perspective from the BRAHMS experiment, *Nucl. Phys. A* **757**, 1 (2005).
- [38] V. Greco, C. M. Ko, and R. Rapp, Quark coalescence for charmed mesons in ultrarelativistic heavy ion collisions, *Phys. Lett. B* **595**, 202 (2004).
- [39] Y. Oh, C. M. Ko, S. H. Lee, and S. Yasui, Heavy baryon/meson ratios in relativistic heavy ion collisions, *Phys. Rev. C* **79**, 044905 (2009).
- [40] J. Adam *et al.* (STAR Collaboration), Observation of Enhancement of Charmed Baryon-To-Meson Ratio in Au+Au Collisions at $\sqrt{s_{NN}} = 200$ GeV, *Phys. Rev. Lett.* **124**, 172301 (2020).
- [41] S. Acharya *et al.* (ALICE Collaboration), Λ_c^+ production in Pb-Pb collisions at $\sqrt{s_{NN}} = 5.02$ TeV, *Phys. Lett. B* **793**, 212 (2019).
- [42] S. H. Lee, K. Ohnishi, S. Yasui, I.-K. Yoo, and C.-M. Ko, Λ_c Enhancement from Strongly Coupled Quark-Gluon Plasma, *Phys. Rev. Lett.* **100**, 222301 (2008).
- [43] J. Zhao, S. Shi, N. Xu, and P. Zhuang, Sequential coalescence with charm conservation in high energy nuclear collisions, [arXiv:1805.10858](https://arxiv.org/abs/1805.10858).
- [44] S. Cho, K.-J. Sun, C. M. Ko, S. H. Lee, and Y. Oh, Charmed hadron production in an improved quark coalescence model, *Phys. Rev. C* **101**, 024909 (2020).
- [45] M. He and R. Rapp, Hadronization and Charm-Hadron Ratios in Heavy-Ion Collisions, *Phys. Rev. Lett.* **124**, 042301 (2020).
- [46] M. Arneodo, Nuclear effects in structure functions, *Phys. Rep.* **240**, 301 (1994).
- [47] S. Malace, D. Gaskell, D. W. Higinbotham, and I. Cloet, The challenge of the EMC Effect: Existing data and future directions, *Int. J. Mod. Phys. E* **23**, 1430013 (2014).
- [48] K. J. Eskola, P. Paakkinen, H. Paukkunen, and C. A. Salgado, EPPS16: Nuclear parton distributions with LHC data, *Eur. Phys. J. C* **77**, 163 (2017).
- [49] K. Kovarik *et al.*, nCTEQ15—Global analysis of nuclear parton distributions with uncertainties in the CTEQ framework, *Phys. Rev. D* **93**, 085037 (2016).
- [50] F. Gelis, E. Iancu, J. Jalilian-Marian, and R. Venugopalan, The color glass condensate, *Annu. Rev. Nucl. Part. Sci.* **60**, 463 (2010).
- [51] P. Tribedy and R. Venugopalan, QCD saturation at the LHC: Comparisons of models to $p + p$ and $A + A$ data and predictions for $p + Pb$ collisions, *Phys. Lett. B* **710**, 125 (2012); **718**, 1154 (2013).
- [52] J. L. Albacete, A. Dumitru, H. Fujii, and Y. Nara, CGC predictions for $p + Pb$ collisions at the LHC, *Nucl. Phys. A* **897**, 1 (2013).
- [53] A. H. Rezaeian, CGC predictions for $p+A$ collisions at the LHC and signature of QCD saturation, *Phys. Lett. B* **718**, 1058 (2013).
- [54] H. Fujii and K. Watanabe, Heavy quark pair production in high energy pA collisions: Open heavy flavors, *Nucl. Phys. A* **920**, 78 (2013).
- [55] I. Vitev, Non-Abelian energy loss in cold nuclear matter, *Phys. Rev. C* **75**, 064906 (2007).
- [56] M. Lev and B. Petersson, Nuclear effects at large transverse momentum in a QCD parton model, *Z. Phys. C* **21**, 155 (1983).
- [57] X.-N. Wang, Systematic study of high p_T hadron spectra in pp , pA , and AA collisions from SPS to RHIC energies, *Phys. Rev. C* **61**, 064910 (2000).
- [58] B. Z. Kopeliovich, J. Nemchik, A. Schafer, and A. V. Tarasov, Cronin Effect in Hadron Production Off Nuclei, *Phys. Rev. Lett.* **88**, 232303 (2002).
- [59] C. Bierlich, T. Sjöstrand, and M. Utheim, Hadronic rescattering in pA and AA collisions, *Eur. Phys. J. A* **57**, 227 (2021).
- [60] A. Beraudo, A. De Pace, M. Monteno, M. Nardi, and F. Prino, Heavy-flavor production in high-energy d-Au and p -Pb collisions, *J. High Energy Phys.* **03** (2016) 123.
- [61] Y. Xu, S. Cao, M. Nahrgang, W. Ke, G.-Y. Qin, J. Auvinen, and S. A. Bass, Heavy-flavor dynamics in relativistic p -Pb collisions at $\sqrt{s_{NN}} = 5.02$ TeV, *Nucl. Part. Phys. Proc.* **276-278**, 225 (2016).
- [62] S. Chatrchyan *et al.* (CMS Collaboration), Observation of long-range near-side angular correlations in proton-lead collisions at the LHC, *Phys. Lett. B* **718**, 795 (2013).
- [63] B. Abelev *et al.* (ALICE Collaboration), Long-range angular correlations on the near and away side in p -Pb collisions at $\sqrt{s_{NN}} = 5.02$ TeV, *Phys. Lett. B* **719**, 29 (2013).
- [64] B. Abelev *et al.* (ALICE Collaboration), Long-range angular correlations of π , K , and p in p -Pb collisions at $\sqrt{s_{NN}} = 5.02$ TeV, *Phys. Lett. B* **726**, 164 (2013).

- [65] J. Adam *et al.* (ALICE Collaboration), Forward-central two-particle correlations in p -Pb collisions at $\sqrt{s_{NN}} = 5.02$ TeV, *Phys. Lett. B* **753**, 126 (2016).
- [66] S. Acharya *et al.* (ALICE Collaboration), Multiplicity dependence of light-flavor hadron production in pp collisions at $\sqrt{s} = 7$ TeV, *Phys. Rev. C* **99**, 024906 (2019).
- [67] S. Acharya *et al.* (ALICE Collaboration), Multiplicity dependence of π , K , and p production in pp collisions at $\sqrt{s} = 13$ TeV, *Eur. Phys. J. C* **80**, 693 (2020).
- [68] J. Adam *et al.* (ALICE Collaboration), Multiplicity dependence of charged pion, kaon, and (anti)proton production at large transverse momentum in p -Pb collisions at $\sqrt{s_{NN}} = 5.02$ TeV, *Phys. Lett. B* **760**, 720 (2016).
- [69] J. L. Nagle and W. A. Zajc, Small system collectivity in relativistic hadronic and nuclear collisions, *Annu. Rev. Nucl. Part. Sci.* **68**, 211 (2018).
- [70] K. J. Eskola, H. Paukkunen, and C. A. Salgado, EPS09: A new generation of NLO and LO nuclear parton distribution functions, *J. High Energy Phys.* **04** (2009) 065.
- [71] R. Aaij *et al.* (LHCb Collaboration), Prompt Λ_c^+ production in p Pb collisions at $\sqrt{s_{NN}} = 5.02$ TeV, *J. High Energy Phys.* **02** (2019) 102.
- [72] M. He and R. Rapp, Charm-baryon production in proton-proton collisions, *Phys. Lett. B* **795**, 117 (2019).
- [73] J. Song, H.-h. Li, and F.-l. Shao, New feature of low p_T charm quark hadronization in pp collisions at $\sqrt{s} = 7$ TeV, *Eur. Phys. J. C* **78**, 344 (2018).
- [74] H.-H. Li, F.-L. Shao, J. Song, and R.-Q. Wang, Production of single-charm hadrons by quark combination mechanism in p -Pb collisions at $\sqrt{s_{NN}} = 5.02$ TeV, *Phys. Rev. C* **97**, 064915 (2018).
- [75] S. Acharya *et al.* (ALICE Collaboration), Measurement of D -meson production at mid-rapidity in pp collisions at $\sqrt{s} = 7$ TeV, *Eur. Phys. J. C* **77**, 550 (2017).
- [76] J. Adam *et al.* (ALICE Collaboration), D -meson production in p -Pb collisions at $\sqrt{s_{NN}} = 5.02$ TeV and in pp collisions at $\sqrt{s} = 7$ TeV, *Phys. Rev. C* **94**, 054908 (2016).
- [77] S. Acharya *et al.* (ALICE Collaboration), Measurement of D^0 , D^+ , D^{*+} , and D_s^+ production in Pb-Pb collisions at $\sqrt{s_{NN}} = 5.02$ TeV, *J. High Energy Phys.* **10** (2018) 174.
- [78] B. Abelev *et al.* (ALICE Collaboration), Measurement of charm production at central rapidity in proton-proton collisions at $\sqrt{s} = 7$ TeV, *J. High Energy Phys.* **01** (2012) 128.
- [79] B. Abelev *et al.* (ALICE Collaboration), D_s^+ meson production at central rapidity in proton-proton collisions at $\sqrt{s} = 7$ TeV, *Phys. Lett. B* **718**, 279 (2012).
- [80] B. Abelev *et al.* (ALICE Collaboration), Measurement of charm production at central rapidity in proton-proton collisions at $\sqrt{s} = 2.76$ TeV, *J. High Energy Phys.* **07** (2012) 191.
- [81] S. Acharya *et al.* (ALICE Collaboration), Λ_c^+ Production and Baryon-to-Meson Ratios in pp and p -Pb Collisions at $\sqrt{s_{NN}} = 5.02$ TeV at the LHC, *Phys. Rev. Lett.* **127**, 202301 (2021).
- [82] K. Aamodt *et al.* (ALICE Collaboration), The ALICE experiment at the CERN LHC, *JINST* **3**, S08002 (2008).
- [83] B. Abelev *et al.* (ALICE Collaboration), Performance of the ALICE experiment at the CERN LHC, *Int. J. Mod. Phys. A* **29**, 1430044 (2014).
- [84] K. Aamodt *et al.* (ALICE Collaboration), Alignment of the ALICE inner tracking system with cosmic-ray tracks, *J. Instrument.* **5**, P03003 (2010).
- [85] J. Alme *et al.*, The ALICE TPC, a large 3-dimensional tracking device with fast readout for ultra-high multiplicity events, *Nucl. Instrum. Meth. A* **622**, 316 (2010).
- [86] J. Adam *et al.* (ALICE Collaboration), Determination of the event collision time with the ALICE detector at the LHC, *Eur. Phys. J. Plus* **132**, 99 (2017).
- [87] S. Acharya *et al.* (ALICE Collaboration), ALICE 2017 luminosity determination for pp collisions at $\sqrt{s} = 5$ TeV. Retrieved from <https://cds.cern.ch/record/2648933>.
- [88] B. Abelev *et al.* (ALICE Collaboration), Measurement of visible cross sections in proton-lead collisions at $\sqrt{s_{NN}} = 5.02$ TeV in van der Meer scans with the ALICE detector, *J. Instrument.* **9**, P11003 (2014).
- [89] P. A. Zyla *et al.* (Particle Data Group Collaboration), Review of particle physics, *Prog. Theor. Exp. Phys.* **2020**, 083C01 (2020).
- [90] J. Adam *et al.* (ALICE Collaboration), Particle identification in ALICE: A Bayesian approach, *Eur. Phys. J. Plus* **131**, 168 (2016).
- [91] H. Voss, A. Höcker, J. Stelzer, and F. Tegenfeldt, TMVA, the toolkit for multivariate data analysis with ROOT, *PoS ACAT*, 040 (2007).
- [92] T. Sjöstrand, S. Mrenna, and P. Z. Skands, PYTHIA 6.4 physics and manual, *J. High Energy Phys.* **05** (2006) 026.
- [93] P. Z. Skands, The Perugia Tunes, in *Proceedings of the 1st International Workshop on Multiple Partonic Interactions at the LHC (MPI'08): Perugia, Italy, October 27–31, 2008* (DESY, Hamburg, Germany, 2009), pp. 284–297.
- [94] X.-N. Wang and M. Gyulassy, HIJING: A Monte Carlo model for multiple jet production in pp , pA , and AA collisions, *Phys. Rev. D* **44**, 3501 (1991).
- [95] T. Sjöstrand, S. Mrenna, and P. Skands, A brief introduction to PYTHIA 8.1, *Comput. Phys. Commun.* **178**, 852 (2008).
- [96] S. Frixione, P. Nason, and G. Ridolfi, A Positive-weight next-to-leading-order Monte Carlo for heavy-flavor hadroproduction, *J. High Energy Phys.* **09** (2007) 126.
- [97] S. Dulat, T.-J. Hou, J. Gao, M. Guzzi, J. Huston, P. Nadolsky, J. Pumplin, C. Schmidt, D. Stump, and C. P. Yuan, New parton distribution functions from a global analysis of quantum chromodynamics, *Phys. Rev. D* **93**, 033006 (2016).
- [98] B. A. Kniehl, G. Kramer, I. Schienbein, and H. Spiesberger, Λ_c^\pm production in pp collisions with a new fragmentation function, *Phys. Rev. D* **101**, 114021 (2020).
- [99] G. Alexander *et al.* (OPAL Collaboration), A Study of charm hadron production in $Z^0 \rightarrow c\bar{c}$ and $Z^0 \rightarrow b\bar{b}$ decays at LEP, *Z. Phys. C* **72**, 1 (1996).
- [100] M. Niiyama *et al.* (Belle Collaboration), Production cross sections of hyperons and charmed baryons from e^+e^- annihilation near $\sqrt{s} = 10.52$ GeV, *Phys. Rev. D* **97**, 072005 (2018).
- [101] S. Acharya *et al.* (ALICE Collaboration), Measurement of prompt D^0 , D^+ , D^{*+} , and D_s^+ production in p -Pb collisions at $\sqrt{s_{NN}} = 5.02$ TeV, *J. High Energy Phys.* **12** (2019) 092.
- [102] C. Bierlich, G. Gustafson, L. Lönnblad, and A. Tarasov, Effects of overlapping strings in pp collisions, *J. High Energy Phys.* **03** (2015) 148.
- [103] D. Ebert, R. N. Faustov, and V. O. Galkin, Spectroscopy and Regge trajectories of heavy baryons in the relativistic quark-diquark picture, *Phys. Rev. D* **84**, 014025 (2011).
- [104] V. Minissale, S. Plumari, and V. Greco, Charm hadrons in pp collisions at LHC energy within a coalescence plus fragmentation approach, *Phys. Lett. B* **821**, 136622 (2021).

- [105] S. Plumari, V. Minissale, S. K. Das, G. Coci, and V. Greco, Charmed hadrons from coalescence plus fragmentation in relativistic nucleus-nucleus collisions at RHIC and LHC, *Eur. Phys. J. C* **78**, 348 (2018).
- [106] S. Acharya *et al.* (ALICE Collaboration), Production of charged pions, kaons, and (anti)protons in Pb-Pb and inelastic pp collisions at $\sqrt{s_{NN}} = 5.02$ TeV, *Phys. Rev. C* **101**, 044907 (2020).
- [107] B. B. Abelev *et al.* (ALICE Collaboration), K_S^0 and Λ Production in Pb-Pb collisions at $\sqrt{s_{NN}} = 2.76$ TeV, *Phys. Rev. Lett.* **111**, 222301 (2013).
- [108] B. Abelev *et al.* (ALICE Collaboration), Multiplicity dependence of pion, kaon, proton, and lambda production in p -Pb collisions at $\sqrt{s_{NN}} = 5.02$ TeV, *Phys. Lett. B* **728**, 25 (2014).
- [109] B. Abelev *et al.* (ALICE Collaboration), Upgrade of the ALICE experiment: Letter of intent, *J. Phys. G* **41**, 087001 (2014).

S. Acharya,¹⁴² D. Adamová,⁹⁷ A. Adler,⁷⁵ J. Adolfsson,⁸² G. Aglieri Rinella,³⁵ M. Agnello,³¹ N. Agrawal,⁵⁵ Z. Ahammed,¹⁴² S. Ahmad,¹⁶ S. U. Ahn,⁷⁷ Z. Akbar,⁵² A. Akindinov,⁹⁴ M. Al-Turany,¹⁰⁹ D. S. D. Albuquerque,¹²⁴ D. Aleksandrov,⁹⁰ B. Alessandro,⁶⁰ H. M. Alfanda,⁷ R. Alfaro Molina,⁷² B. Ali,¹⁶ Y. Ali,¹⁴ A. Alici,²⁶ N. Alizadehvandchali,¹²⁷ A. Alkin,³⁵ J. Alme,²¹ T. Alt,⁶⁹ L. Altenkamper,²¹ I. Altsybeev,¹¹⁵ M. N. Anaam,⁷ C. Andrei,⁴⁹ D. Andreou,⁹² A. Andronic,¹⁴⁵ M. Angeletti,³⁵ V. Anguelov,¹⁰⁶ T. Antičić,¹¹⁰ F. Antinori,⁵⁸ P. Antonioli,⁵⁵ N. Apadula,⁸¹ L. Aphecetche,¹¹⁷ H. Appelshäuser,⁶⁹ S. Arcelli,²⁶ R. Arnaldi,⁶⁰ M. Arratia,⁸¹ I. C. Arsene,²⁰ M. Arslanodok,^{147,106} A. Augustinus,³⁵ R. Averbeck,¹⁰⁹ S. Aziz,⁷⁹ M. D. Azmi,¹⁶ A. Badalà,⁵⁷ Y. W. Baek,⁴² X. Bai,¹⁰⁹ R. Bailhache,⁶⁹ R. Bala,¹⁰³ A. Balbino,³¹ A. Baldisseri,¹³⁹ M. Ball,⁴⁴ D. Banerjee,⁴ R. Barbera,²⁷ L. Barioglio,²⁵ M. Barlou,⁸⁶ G. G. Barnaföldi,¹⁴⁶ L. S. Barnby,⁹⁶ V. Barret,¹³⁶ C. Bartels,¹²⁹ K. Barth,³⁵ E. Bartsch,⁶⁹ F. Baruffaldi,²⁸ N. Bastid,¹³⁶ S. Basu,^{82,144} G. Batigne,¹¹⁷ B. Batyunya,⁷⁶ D. Bauri,⁵⁰ J. L. Bazo Alba,¹¹⁴ I. G. Bearden,⁹¹ C. Beattie,¹⁴⁷ I. Belikov,¹³⁸ A. D. C. Bell Hechavarria,¹⁴⁵ F. Bellini,³⁵ R. Bellwied,¹²⁷ S. Belokurova,¹¹⁵ V. Belyaev,⁹⁵ G. Bencedi,^{70,146} S. Beole,²⁵ A. Bercuci,⁴⁹ Y. Berdnikov,¹⁰⁰ A. Berdnikova,¹⁰⁶ D. Berenyi,¹⁴⁶ L. Bergmann,¹⁰⁶ M. G. Besoiu,⁶⁸ L. Betev,³⁵ P. P. Bhaduri,¹⁴² A. Bhasin,¹⁰³ I. R. Bhat,¹⁰³ M. A. Bhat,⁴ B. Bhattacharjee,⁴³ P. Bhattacharya,²³ A. Bianchi,²⁵ L. Bianchi,²⁵ N. Bianchi,⁵³ J. Bielčák,³⁸ J. Bielčíková,⁹⁷ A. Bilandzic,¹⁰⁷ G. Biro,¹⁴⁶ S. Biswas,⁴ J. T. Blair,¹²¹ D. Blau,⁹⁰ M. B. Blidaru,¹⁰⁹ C. Blume,⁶⁹ G. Boca,²⁹ F. Bock,⁹⁸ A. Bogdanov,⁹⁵ S. Boi,²³ J. Bok,⁶² L. Boldizsár,¹⁴⁶ A. Bolozdynya,⁹⁵ M. Bombara,³⁹ G. Bonomi,¹⁴¹ H. Borel,¹³⁹ A. Borissov,^{83,95} H. Bossi,¹⁴⁷ E. Botta,²⁵ L. Bratrud,⁶⁹ P. Braun-Munzinger,¹⁰⁹ M. Bregant,¹²³ M. Broz,³⁸ G. E. Bruno,^{108,34} M. D. Buckland,¹²⁹ D. Budnikov,¹¹¹ H. Buesching,⁶⁹ S. Bufalino,³¹ O. Bugnon,¹¹⁷ P. Buhler,¹¹⁶ P. Buncic,³⁵ Z. Buthelezi,^{73,133} J. B. Butt,¹⁴ S. A. Bysiak,¹²⁰ D. Caffarri,⁹² M. Cai,⁷ A. Caliva,¹⁰⁹ E. Calvo Villar,¹¹⁴ J. M. M. Camacho,¹²² R. S. Camacho,⁴⁶ P. Camerini,²⁴ F. D. M. Canedo,¹²³ A. A. Capon,¹¹⁶ F. Carnesecchi,²⁶ R. Caron,¹³⁹ J. Castillo Castellanos,¹³⁹ E. A. R. Casula,⁵⁶ F. Catalano,³¹ C. Ceballos Sanchez,⁷⁶ P. Chakraborty,⁵⁰ S. Chandra,¹⁴² W. Chang,⁷ S. Chapeland,³⁵ M. Chartier,¹²⁹ S. Chattopadhyay,¹⁴² S. Chattopadhyay,¹¹² A. Chauvin,²³ C. Cheshkov,¹³⁷ B. Cheynis,¹³⁷ V. Chibante Barroso,³⁵ D. D. Chinellato,¹²⁴ S. Cho,⁶² P. Chochula,³⁵ P. Christakoglou,⁹² C. H. Christensen,⁹¹ P. Christiansen,⁸² T. Chujo,¹³⁵ C. Cicalo,⁵⁶ L. Cifarelli,²⁶ F. Cindolo,⁵⁵ M. R. Ciupek,¹⁰⁹ G. Clai,^{55,a} J. Cleymans,¹²⁶ F. Colamaria,⁵⁴ J. S. Colburn,¹¹³ D. Colella,⁵⁴ A. Collu,⁸¹ M. Colocci,^{35,26} M. Concas,^{60,b} G. Conesa Balbastre,⁸⁰ Z. Conesa del Valle,⁷⁹ G. Contin,²⁴ J. G. Contreras,³⁸ T. M. Cormier,⁹⁸ P. Cortese,³² M. R. Cosentino,¹²⁵ F. Costa,³⁵ S. Costanza,²⁹ P. Crochet,¹³⁶ E. Cuautle,⁷⁰ P. Cui,⁷ L. Cunqueiro,⁹⁸ T. Dahms,¹⁰⁷ A. Dainese,⁵⁸ F. P. A. Damas,^{117,139} M. C. Danisch,¹⁰⁶ A. Danu,⁶⁸ D. Das,¹¹² I. Das,¹¹² P. Das,⁸⁸ P. Das,⁴ S. Das,⁴ S. Dash,⁵⁰ S. De,⁸⁸ A. De Caro,³⁰ G. de Cataldo,⁵⁴ L. De Cilladi,²⁵ J. de Cuveland,⁴⁰ A. De Falco,²³ D. De Gruttola,³⁰ N. De Marco,⁶⁰ C. De Martin,²⁴ S. De Pasquale,³⁰ S. Deb,⁵¹ H. F. Degenhardt,¹²³ K. R. Deja,¹⁴³ S. Delsanto,²⁵ W. Deng,⁷ P. Dhankher,^{19,50} D. Di Bari,³⁴ A. Di Mauro,³⁵ R. A. Diaz,⁸ T. Dietel,¹²⁶ P. Dillenseger,⁶⁹ Y. Ding,⁷ R. Divià,³⁵ D. U. Dixit,¹⁹ Ø. Djuvnsland,²¹ U. Dmitrieva,⁶⁴ J. Do,⁶² A. Dobrin,⁶⁸ B. Dönigus,⁶⁹ O. Dordic,²⁰ A. K. Dubey,¹⁴² A. Dubla,^{109,92} S. Dudi,¹⁰² M. Dukhishyam,⁸⁸ P. Dupieux,¹³⁶ T. M. Eder,¹⁴⁵ R. J. Ehlers,⁹⁸ V. N. Eikeland,²¹ D. Elia,⁵⁴ B. Erazmus,¹¹⁷ F. Erhardt,¹⁰¹ A. Erokhin,¹¹⁵ M. R. Ersdal,²¹ B. Espagnon,⁷⁹ G. Eulisse,³⁵ D. Evans,¹¹³ S. Evdokimov,⁹³ L. Fabbietti,¹⁰⁷ M. Faggin,²⁸ J. Faivre,⁸⁰ F. Fan,⁷ A. Fantoni,⁵³ M. Fasel,⁹⁸ P. Fecchio,³¹ A. Feliciello,⁶⁰ G. Feofilov,¹¹⁵ A. Fernández Téllez,⁴⁶ A. Ferrero,¹³⁹ A. Ferretti,²⁵ A. Festanti,³⁵ V. J. G. Feuillard,¹⁰⁶ J. Figiel,¹²⁰ S. Filchagin,¹¹¹ D. Finogeev,⁶⁴ F. M. Fionda,²¹ G. Fiorenza,⁵⁴ F. Flor,¹²⁷ A. N. Flores,¹²¹ S. Foertsch,⁷³ P. Foka,¹⁰⁹ S. Fokin,⁹⁰ E. Fragiaco,⁶¹ U. Fuchs,³⁵ C. Furget,⁸⁰ A. Furs,⁶⁴ M. Fusco Girard,³⁰ J. J. Gaardhøje,⁹¹ M. Gagliardi,²⁵ A. M. Gago,¹¹⁴ A. Gal,¹³⁸ C. D. Galvan,¹²² P. Ganoti,⁸⁶ C. Garabatos,¹⁰⁹ J. R. A. Garcia,⁴⁶ E. Garcia-Solis,¹⁰ K. Garg,¹¹⁷ C. Gargiulo,³⁵ A. Garibli,⁸⁹ K. Garner,¹⁴⁵ P. Gasik,¹⁰⁷ E. F. Gauger,¹²¹ M. B. Gay Ducati,⁷¹ M. Germain,¹¹⁷ J. Ghosh,¹¹² P. Ghosh,¹⁴² S. K. Ghosh,⁴ M. Giacalone,²⁶ P. Gianotti,⁵³ P. Giubellino,^{109,60} P. Giubilato,²⁸ A. M. C. Glaenger,¹³⁹ P. Glässel,¹⁰⁶ V. Gonzalez,¹⁴⁴ L. H. González-Trueba,⁷² S. Gorbunov,⁴⁰ L. Görlich,¹²⁰ S. Gotovac,³⁶ V. Grabski,⁷² L. K. Graczykowski,¹⁴³ K. L. Graham,¹¹³ L. Greiner,⁸¹ A. Grelli,⁶³ C. Grigoras,³⁵ V. Grigoriev,⁹⁵ A. Grigoryan,^{1,c} S. Grigoryan,⁷⁶ O. S. Groettvik,²¹ F. Grosa,⁶⁰ J. F. Grosse-Oetringhaus,³⁵ R. Grosso,¹⁰⁹ R. Guernane,⁸⁰ M. Guilbaud,¹¹⁷ M. Guittiere,¹¹⁷ K. Gulbrandsen,⁹¹ T. Gunji,¹³⁴ A. Gupta,¹⁰³ R. Gupta,¹⁰³ I. B. Guzman,⁴⁶ R. Haake,¹⁴⁷ M. K. Habib,¹⁰⁹ C. Hadjidakis,⁷⁹ H. Hamagaki,⁸⁴ G. Hamar,¹⁴⁶ M. Hamid,⁷ R. Hannigan,¹²¹ M. R. Haque,^{143,88} A. Harlenderova,¹⁰⁹ J. W. Harris,¹⁴⁷ A. Harton,¹⁰ J. A. Hasenbichler,³⁵ H. Hassan,⁹⁸ D. Hatzifotiadou,⁵⁵ P. Hauer,⁴⁴ L. B. Havener,¹⁴⁷ S. Hayashi,¹³⁴ S. T. Heckel,¹⁰⁷ E. Hellbär,⁶⁹ H. Helstrup,³⁷ T. Herman,³⁸ E. G. Hernandez,⁴⁶ G. Herrera Corral,⁹ F. Herrmann,¹⁴⁵ K. F. Hetland,³⁷ H. Hillemanns,³⁵ C. Hills,¹²⁹ B. Hippolyte,¹³⁸ B. Hohlweger,¹⁰⁷ J. Honermann,¹⁴⁵ G. H. Hong,¹⁴⁸ D. Horak,³⁸

- S. Hornung,¹⁰⁹ R. Hosokawa,¹⁵ P. Hristov,³⁵ C. Huang,⁷⁹ C. Hughes,¹³² P. Huhn,⁶⁹ T. J. Humanic,⁹⁹ H. Hushnud,¹¹² L. A. Husova,¹⁴⁵ N. Hussain,⁴³ D. Hutter,⁴⁰ J. P. Iddon,^{35,129} R. Ilkaev,¹¹¹ H. Ilyas,¹⁴ M. Inaba,¹³⁵ G. M. Innocenti,³⁵ M. Ippolitov,⁹⁰ A. Isakov,^{38,97} M. S. Islam,¹¹² M. Ivanov,¹⁰⁹ V. Ivanov,¹⁰⁰ V. Izucheev,⁹³ B. Jacak,⁸¹ N. Jacazio,^{35,55} P. M. Jacobs,⁸¹ S. Jadlovsky,¹¹⁹ J. Jadlovsky,¹¹⁹ S. Jaelani,⁶³ C. Jahnke,¹²³ M. J. Jakubowska,¹⁴³ M. A. Janik,¹⁴³ T. Janson,⁷⁵ M. Jercic,¹⁰¹ O. Jevons,¹¹³ M. Jin,¹²⁷ F. Jonas,^{98,145} P. G. Jones,¹¹³ J. Jung,⁶⁹ M. Jung,⁶⁹ A. Jusko,¹¹³ P. Kalinik,⁶⁵ A. Kalweit,³⁵ V. Kaplin,⁹⁵ S. Kar,⁷ A. Karasu Uysal,⁷⁸ D. Karatovic,¹⁰¹ O. Karavichev,⁶⁴ T. Karavicheva,⁶⁴ P. Karczmarczyk,¹⁴³ E. Karpechev,⁶⁴ A. Kazantsev,⁹⁰ U. Kebschull,⁷⁵ R. Keidel,⁴⁸ M. Keil,³⁵ B. Ketzer,⁴⁴ Z. Khabanova,⁹² A. M. Khan,⁷ S. Khan,¹⁶ A. Khanzadeev,¹⁰⁰ Y. Kharlov,⁹³ A. Khatun,¹⁶ A. Khuntia,¹²⁰ B. Kileng,³⁷ B. Kim,⁶² D. Kim,¹⁴⁸ D. J. Kim,¹²⁸ E. J. Kim,⁷⁴ H. Kim,¹⁷ J. Kim,¹⁴⁸ J. S. Kim,⁴² J. Kim,¹⁰⁶ J. Kim,¹⁴⁸ J. Kim,⁷⁴ M. Kim,¹⁰⁶ S. Kim,¹⁸ T. Kim,¹⁴⁸ T. Kim,¹⁴⁸ S. Kirsch,⁶⁹ I. Kisel,⁴⁰ S. Kiselev,⁹⁴ A. Kisiel,¹⁴³ J. L. Klay,⁶ J. Klein,^{35,60} S. Klein,⁸¹ C. Klein-Bösing,¹⁴⁵ M. Kleiner,⁶⁹ T. Klemenzt,¹⁰⁷ A. Kluge,³⁵ A. G. Knospe,¹²⁷ C. Kobdaj,¹¹⁸ M. K. Köhler,¹⁰⁶ T. Kollegger,¹⁰⁹ A. Kondratyev,⁷⁶ N. Kondratyeva,⁹⁵ E. Kondratyuk,⁹³ J. König,⁶⁹ S. A. Königstorfer,¹⁰⁷ P. J. Konopka,^{2,35} G. Kornakov,¹⁴³ S. D. Koryciak,² L. Koska,¹¹⁹ O. Kovalenko,⁸⁷ V. Kovalenko,¹¹⁵ M. Kowalski,¹²⁰ I. Králik,⁶⁵ A. Kravčáková,³⁹ L. Kreis,¹⁰⁹ M. Krivda,^{113,65} F. Krizek,⁹⁷ K. Krizkova Gajdosova,³⁸ M. Kroesen,¹⁰⁶ M. Krüger,⁶⁹ E. Kryshen,¹⁰⁰ M. Krzewicki,⁴⁰ V. Kučera,³⁵ C. Kuhn,¹³⁸ P. G. Kuijper,⁹² T. Kumaoka,¹³⁵ L. Kumar,¹⁰² S. Kundu,⁸⁸ P. Kurashvili,⁸⁷ A. Kurepin,⁶⁴ A. B. Kurepin,⁶⁴ A. Kuryakin,¹¹¹ S. Kushpil,⁹⁷ J. Kvapil,¹¹³ M. J. Kweon,⁶² J. Y. Kwon,⁶² Y. Kwon,¹⁴⁸ S. L. La Pointe,⁴⁰ P. La Rocca,²⁷ Y. S. Lai,⁸¹ A. Lakrathok,¹¹⁸ M. Lamanna,³⁵ R. Langoy,¹³¹ K. Lapidus,³⁵ P. Larionov,⁵³ E. Laudi,³⁵ L. Lautner,³⁵ R. Lavicka,³⁸ T. Lazareva,¹¹⁵ R. Lea,²⁴ J. Lee,¹³⁵ S. Lee,¹⁴⁸ J. Leibrach,⁴⁰ R. C. Lemmon,⁹⁶ I. León Monzón,¹²² E. D. Lesser,¹⁹ M. Lettrich,³⁵ P. Lévai,¹⁴⁶ X. Li,¹¹ X. L. Li,⁷ J. Lien,¹³¹ R. Lietava,¹¹³ B. Lim,¹⁷ S. H. Lim,¹⁷ V. Lindenstruth,⁴⁰ A. Lindner,⁴⁹ C. Lippmann,¹⁰⁹ A. Liu,¹⁹ J. Liu,¹²⁹ I. M. Lofnes,²¹ V. Loginov,⁹⁵ C. Loizides,⁹⁸ P. Loncar,³⁶ J. A. Lopez,¹⁰⁶ X. Lopez,¹³⁶ E. López Torres,⁸ J. R. Luhder,¹⁴⁵ M. Lunardon,²⁸ G. Luparello,⁶¹ Y. G. Ma,⁴¹ A. Maevskaya,⁶⁴ M. Mager,³⁵ S. M. Mahmood,²⁰ T. Mahmoud,⁴⁴ A. Maire,¹³⁸ R. D. Majka,¹⁴⁷ M. Malaev,¹⁰⁰ Q. W. Malik,²⁰ L. Malinina,^{76,d} D. Mal'Kevich,⁹⁴ N. Mallick,⁵¹ P. Malzacher,¹⁰⁹ G. Mandaglio,^{33,57} V. Manko,⁹⁰ F. Manso,¹³⁶ V. Manzari,⁵⁴ Y. Mao,⁷ M. Marchisone,¹³⁷ J. Mareš,⁶⁷ G. V. Margagliotti,²⁴ A. Margotti,⁵⁵ A. Marín,¹⁰⁹ C. Markert,¹²¹ M. Marquard,⁶⁹ N. A. Martin,¹⁰⁶ P. Martinengo,³⁵ J. L. Martínez,¹²⁷ M. I. Martínez,⁴⁶ G. Martínez García,¹¹⁷ S. Masciocchi,¹⁰⁹ M. Maserà,²⁵ A. Masoni,⁵⁶ L. Massacrier,⁷⁹ A. Mastroserio,^{140,54} A. M. Mathis,¹⁰⁷ O. Matonoha,⁸² P. F. T. Matuoka,¹²³ A. Matyja,¹²⁰ C. Mayer,¹²⁰ F. Mazzaschi,²⁵ M. Mazzilli,⁵⁴ M. A. Mazzoni,⁵⁹ A. F. Mechler,⁶⁹ F. Meddi,²² Y. Melikyan,⁶⁴ A. Menchaca-Rocha,⁷² E. Meninno,^{116,30} A. S. Menon,¹²⁷ M. Meres,¹³ S. Mhlanga,¹²⁶ Y. Miaske,¹³⁵ L. Micheletti,²⁵ L. C. Migliorin,¹³⁷ D. L. Mihaylov,¹⁰⁷ K. Mikhaylov,^{76,94} A. N. Mishra,^{146,70} D. Miśkowiec,¹⁰⁹ A. Modak,⁴ N. Mohammadi,³⁵ A. P. Mohanty,⁶³ B. Mohanty,⁸⁸ M. Mohisin Khan,¹⁶ Z. Moravcova,⁹¹ C. Mordasini,¹⁰⁷ D. A. Moreira De Godoy,¹⁴⁵ L. A. P. Moreno,⁴⁶ I. Morozov,⁶⁴ A. Morsch,³⁵ T. Mrnjavac,³⁵ V. Muccifora,⁵³ E. Mudnic,³⁶ D. Mühlheim,¹⁴⁵ S. Muhuri,¹⁴² J. D. Mulligan,⁸¹ A. Mulliri,^{23,56} M. G. Munhoz,¹²³ R. H. Munzer,⁶⁹ H. Murakami,¹³⁴ S. Murray,¹²⁶ L. Musa,³⁵ J. Musinsky,⁶⁵ C. J. Myers,¹²⁷ J. W. Myrcha,¹⁴³ B. Naik,⁵⁰ R. Nair,⁸⁷ B. K. Nandi,⁵⁰ R. Nania,⁵⁵ E. Nappi,⁵⁴ M. U. Naru,¹⁴ A. F. Nassirpour,⁸² C. Natrass,¹³² R. Nayak,⁵⁰ S. Nazarenko,¹¹¹ A. Neagu,²⁰ L. Nellen,⁷⁰ S. V. Nesbo,³⁷ G. Neskovic,⁴⁰ D. Nesterov,¹¹⁵ B. S. Nielsen,⁹¹ S. Nikolaev,⁹⁰ S. Nikulin,⁹⁰ V. Nikulin,¹⁰⁰ F. Noferini,⁵⁵ S. Noh,¹² P. Nomokonov,⁷⁶ J. Norman,¹²⁹ N. Novitzky,¹³⁵ P. Nowakowski,¹⁴³ A. Nyanin,⁹⁰ J. Nystrand,²¹ M. Ogino,⁸⁴ A. Ohlson,⁸² J. Oleniacz,¹⁴³ A. C. Oliveira Da Silva,¹³² M. H. Oliver,¹⁴⁷ B. S. Onnerstad,¹²⁸ C. Oppedisano,⁶⁰ A. Ortiz Velasquez,⁷⁰ T. Osako,⁴⁷ A. Oskarsson,⁸² J. Otwinowski,¹²⁰ K. Oyama,⁸⁴ Y. Pachmayer,¹⁰⁶ S. Padhan,⁵⁰ D. Pagano,¹⁴¹ G. Paić,⁷⁰ J. Pan,¹⁴⁴ S. Panebianco,¹³⁹ P. Pareek,¹⁴² J. Park,⁶² J. E. Parkkila,¹²⁸ S. Parmar,¹⁰² S. P. Pathak,¹²⁷ B. Paul,²³ J. Pazzini,¹⁴¹ H. Pei,⁷ T. Peitzmann,⁶³ X. Peng,⁷ L. G. Pereira,⁷¹ H. Pereira Da Costa,¹³⁹ D. Peresunko,⁹⁰ G. M. Perez,⁸ S. Perrin,¹³⁹ Y. Pestov,⁵ V. Petráček,³⁸ M. Petrovici,⁴⁹ R. P. Pezzi,⁷¹ S. Piano,⁶¹ M. Pikna,¹³ P. Pillot,¹¹⁷ O. Pinazza,^{55,35} L. Pinsky,¹²⁷ C. Pinto,²⁷ S. Pisano,⁵³ M. Płoskoń,⁸¹ M. Planinic,¹⁰¹ F. Pliquett,⁶⁹ M. G. Poghosyan,⁹⁸ B. Polichtchouk,⁹³ N. Poljak,¹⁰¹ A. Pop,⁴⁹ S. Porteboeuf-Houssais,¹³⁶ J. Porter,⁸¹ V. Pozdniakov,⁷⁶ S. K. Prasad,⁴ R. Preghenella,⁵⁵ F. Prino,⁶⁰ C. A. Pruneau,¹⁴⁴ I. Pshenichnov,⁶⁴ M. Puccio,³⁵ S. Qiu,⁹² L. Quaglia,²⁵ R. E. Quishpe,¹²⁷ S. Ragoni,¹¹³ J. Rak,¹²⁸ A. Rakotozafindrabe,¹³⁹ L. Ramello,³² F. Rami,¹³⁸ S. A. R. Ramirez,⁴⁶ A. G. T. Ramos,³⁴ R. Raniwala,¹⁰⁴ S. Raniwala,¹⁰⁴ S. S. Räsänen,⁴⁵ R. Rath,⁵¹ I. Ravasenga,⁹² K. F. Read,^{98,132} A. R. Redelbach,⁴⁰ K. Redlich,^{87,e} A. Rehman,²¹ P. Reichelt,⁶⁹ F. Reidt,³⁵ R. Renfordt,⁶⁹ Z. Rescakova,³⁹ K. Reyggers,¹⁰⁶ A. Riabov,¹⁰⁰ V. Riabov,¹⁰⁰ T. Richert,^{82,91} M. Richter,²⁰ P. Riedler,³⁵ W. Riegler,³⁵ F. Riggi,²⁷ C. Ristea,⁶⁸ S. P. Rode,⁵¹ M. Rodríguez Cahuantzi,⁴⁶ K. Røed,²⁰ R. Rogalev,⁹³ E. Rogochaya,⁷⁶ T. S. Rogoschinski,⁶⁹ D. Rohr,³⁵ D. Röhrich,²¹ P. F. Rojas,⁴⁶ P. S. Rokita,¹⁴³ F. Ronchetti,⁵³ A. Rosano,^{33,57} E. D. Rosas,⁷⁰ A. Rossi,⁵⁸ A. Rotondi,²⁹ A. Roy,⁵¹ P. Roy,¹¹² O. V. Rueda,⁸² R. Rui,²⁴ B. Romyantsev,⁷⁶ A. Rustamov,⁸⁹ E. Ryabinkin,⁹⁰ Y. Ryabov,¹⁰⁰ A. Rybicki,¹²⁰ H. Rytkonen,¹²⁸ O. A. M. Saarimäki,⁴⁵ R. Sadek,¹¹⁷ S. Sadosky,⁹³ J. Saetre,²¹ K. Šafařík,³⁸ S. K. Saha,¹⁴² S. Saha,⁸⁸ B. Sahoo,⁵⁰ P. Sahoo,⁵⁰ R. Sahoo,⁵¹ S. Sahoo,⁶⁶ D. Sahu,⁵¹ P. K. Sahu,⁶⁶ J. Saini,¹⁴² S. Sakai,¹³⁵ S. Sambyal,¹⁰³ V. Samsonov,^{100,95} D. Sarkar,¹⁴⁴ N. Sarkar,¹⁴² P. Sarma,⁴³ V. M. Sarti,¹⁰⁷ M. H. P. Sas,^{147,63} J. Schambach,^{98,121} H. S. Scheid,⁶⁹ C. Schiaua,⁴⁹ R. Schicker,¹⁰⁶ A. Schmah,¹⁰⁶ C. Schmidt,¹⁰⁹ H. R. Schmidt,¹⁰⁵ M. O. Schmidt,¹⁰⁶ M. Schmidt,¹⁰⁵ N. V. Schmidt,^{98,69} A. R. Schmier,¹³² R. Schotter,¹³⁸ J. Schukraft,³⁵ Y. Schutz,¹³⁸ K. Schwarz,¹⁰⁹ K. Schweda,¹⁰⁹ G. Scioli,²⁶ E. Scomparin,⁶⁰ J. E. Seger,¹⁵ Y. Sekiguchi,¹³⁴ D. Sekihata,¹³⁴ I. Selyuzhenkov,^{109,95} S. Senyukov,¹³⁸ J. J. Seo,⁶² D. Serebryakov,⁶⁴ L. Šerkšnytė,¹⁰⁷ A. Sevcenco,⁶⁸ A. Shabanov,⁶⁴ A. Shabetai,¹¹⁷ R. Shahoyan,³⁵ W. Shaikh,¹¹² A. Shangaraev,⁹³ A. Sharma,¹⁰² H. Sharma,¹²⁰ M. Sharma,¹⁰³ N. Sharma,¹⁰² S. Sharma,¹⁰³ O. Sheibani,¹²⁷ A. I. Sheikh,¹⁴²

K. Shigaki,⁴⁷ M. Shimomura,⁸⁵ S. Shirinkin,⁹⁴ Q. Shou,⁴¹ Y. Sibiraki,⁹⁰ S. Siddhanta,⁵⁶ T. Siemiarczuk,⁸⁷ D. Silvermyr,⁸² G. Simatovic,⁹² G. Simonetti,³⁵ B. Singh,¹⁰⁷ R. Singh,⁸⁸ R. Singh,¹⁰³ R. Singh,⁵¹ V. K. Singh,¹⁴² V. Singhal,¹⁴² T. Sinha,¹¹² B. Sitar,¹³ M. Sitta,³² T. B. Skaali,²⁰ M. Slupecki,⁴⁵ N. Smirnov,¹⁴⁷ R. J. M. Snellings,⁶³ C. Soncco,¹¹⁴ J. Song,¹²⁷ A. Songmoolnak,¹¹⁸ F. Soramel,²⁸ S. Sorensen,¹³² I. Sputowska,¹²⁰ J. Stachel,¹⁰⁶ I. Stan,⁶⁸ P. J. Steffanic,¹³² S. F. Stiefelmaier,¹⁰⁶ D. Stocco,¹¹⁷ M. M. Stortvedt,³⁷ L. D. Stritto,³⁰ C. P. Stylianidis,⁹² A. A. P. Suaide,¹²³ T. Sugitate,⁴⁷ C. Suire,⁷⁹ M. Suljic,³⁵ R. Sultanov,⁹⁴ M. Šumbera,⁹⁷ V. Sumberia,¹⁰³ S. Sumowidagdo,⁵² S. Swain,⁶⁶ A. Szabo,¹³ I. Szarka,¹³ U. Tabassam,¹⁴ S. F. Taghavi,¹⁰⁷ G. TAILLEPIED,¹³⁶ J. Takahashi,¹²⁴ G. J. Tambave,²¹ S. Tang,^{136,7} Z. Tang,¹³⁰ M. Tarhini,¹¹⁷ M. G. Tarzila,⁴⁹ A. Tauro,³⁵ G. Tejada Muñoz,⁴⁶ A. Telesca,³⁵ L. Terlizzi,²⁵ C. Terrevoli,¹²⁷ G. Tersimonov,³ S. Thakur,¹⁴² D. Thomas,¹²¹ F. Thoresen,⁹¹ R. Tieulent,¹³⁷ A. Tikhonov,⁶⁴ A. R. Timmins,¹²⁷ M. Tkacik,¹¹⁹ A. Toia,⁶⁹ N. Topilskaya,⁶⁴ M. Toppi,⁵³ F. Torales-Acosta,¹⁹ S. R. Torres,^{38,9} A. Trifiró,^{33,57} S. Tripathy,⁷⁰ T. Tripathy,⁵⁰ S. Trogolo,²⁸ G. Trombetta,³⁴ L. Tropp,³⁹ V. Trubnikov,³ W. H. Trzaska,¹²⁸ T. P. Trzcinski,¹⁴³ B. A. Trzeciak,³⁸ A. Tumkin,¹¹¹ R. Turrisi,⁵⁸ T. S. Tsveter,²⁰ K. Ullaland,²¹ E. N. Umaka,¹²⁷ A. Uras,¹³⁷ G. L. Usai,²³ M. Vala,³⁹ N. Valle,²⁹ S. Vallerio,⁶⁰ N. van der Kolk,⁶³ L. V. R. van Doremalen,⁶³ M. van Leeuwen,⁹² P. Vande Vyvre,³⁵ D. Varga,¹⁴⁶ Z. Varga,¹⁴⁶ M. Varga-Kofarago,¹⁴⁶ A. Vargas,⁴⁶ M. Vasileiou,⁸⁶ A. Vasiliev,⁹⁰ O. Vázquez Doce,¹⁰⁷ V. Vechernin,¹¹⁵ E. Vercellin,²⁵ S. Vergara Limón,⁴⁶ L. Vermunt,⁶³ R. Vértesi,¹⁴⁶ M. Verweij,⁶³ L. Vickovic,³⁶ Z. Vilakazi,¹³³ O. Villalobos Baillie,¹¹³ G. VINO,⁵⁴ A. Vinogradov,⁹⁰ T. Virgili,³⁰ V. Vislavicius,⁹¹ A. Vodopyanov,⁷⁶ B. Volkel,³⁵ M. A. Völkl,¹⁰⁵ K. Voloshin,⁹⁴ S. A. Voloshin,¹⁴⁴ G. Volpe,³⁴ B. von Haller,³⁵ I. Vorobyev,¹⁰⁷ D. Voscek,¹¹⁹ J. Vrláková,³⁹ B. Wagner,²¹ M. Weber,¹¹⁶ A. Wegrzynek,³⁵ S. C. Wenzel,³⁵ J. P. Wessels,¹⁴⁵ J. Wiechula,⁶⁹ J. Wikne,²⁰ G. Wilk,⁸⁷ J. Wilkinson,¹⁰⁹ G. A. Willems,¹⁴⁵ E. Willsher,¹¹³ B. Windelband,¹⁰⁶ M. Winn,¹³⁹ W. E. Witt,¹³² J. R. Wright,¹²¹ Y. Wu,¹³⁰ R. Xu,⁷ S. Yalcin,⁷⁸ Y. Yamaguchi,⁴⁷ K. Yamakawa,⁴⁷ S. Yang,²¹ S. Yano,^{47,139} Z. Yin,⁷ H. Yokoyama,⁶³ I.-K. Yoo,¹⁷ J. H. Yoon,⁶² S. Yuan,²¹ A. Yuncu,¹⁰⁶ V. Yurchenko,³ V. Zaccolo,²⁴ A. Zaman,¹⁴ C. Zampolli,³⁵ H. J. C. Zanoli,⁶³ N. Zardoshti,³⁵ A. Zarochentsev,¹¹⁵ P. Závada,⁶⁷ N. Zaviyalov,¹¹¹ H. Zbroszczyk,¹⁴³ M. Zhalov,¹⁰⁰ S. Zhang,⁴¹ X. Zhang,⁷ Y. Zhang,¹³⁰ V. Zhrebchevskii,¹¹⁵ Y. Zhi,¹¹ D. Zhou,⁷ Y. Zhou,⁹¹ J. Zhu,^{7,109} Y. Zhu,⁷ A. Zichichi,²⁶ G. Zinovjev,³ and N. Zurlo¹⁴¹

(ALICE Collaboration)

- ¹A.I. Alikhanyan National Science Laboratory (Yerevan Physics Institute) Foundation, Yerevan, Armenia
²AGH University of Science and Technology, Cracow, Poland
³Bogolyubov Institute for Theoretical Physics, National Academy of Sciences of Ukraine, Kiev, Ukraine
⁴Bose Institute, Department of Physics and Centre for Astroparticle Physics and Space Science (CAPSS), Kolkata, India
⁵Budker Institute for Nuclear Physics, Novosibirsk, Russia
⁶California Polytechnic State University, San Luis Obispo, California, USA
⁷Central China Normal University, Wuhan, China
⁸Centro de Aplicaciones Tecnológicas y Desarrollo Nuclear (CEADEN), Havana, Cuba
⁹Centro de Investigación y de Estudios Avanzados (CINVESTAV), Mexico City and Mérida, Mexico
¹⁰Chicago State University, Chicago, Illinois, USA
¹¹China Institute of Atomic Energy, Beijing, China
¹²Chungbuk National University, Cheongju, Republic of Korea
¹³Comenius University Bratislava, Faculty of Mathematics, Physics and Informatics, Bratislava, Slovakia
¹⁴COMSATS University Islamabad, Islamabad, Pakistan
¹⁵Creighton University, Omaha, Nebraska, USA
¹⁶Department of Physics, Aligarh Muslim University, Aligarh, India
¹⁷Department of Physics, Pusan National University, Pusan, Republic of Korea
¹⁸Department of Physics, Sejong University, Seoul, Republic of Korea
¹⁹Department of Physics, University of California, Berkeley, California, USA
²⁰Department of Physics, University of Oslo, Oslo, Norway
²¹Department of Physics and Technology, University of Bergen, Bergen, Norway
²²Dipartimento di Fisica dell'Università 'La Sapienza' and Sezione INFN, Rome, Italy
²³Dipartimento di Fisica dell'Università and Sezione INFN, Cagliari, Italy
²⁴Dipartimento di Fisica dell'Università and Sezione INFN, Trieste, Italy
²⁵Dipartimento di Fisica dell'Università and Sezione INFN, Turin, Italy
²⁶Dipartimento di Fisica e Astronomia dell'Università and Sezione INFN, Bologna, Italy
²⁷Dipartimento di Fisica e Astronomia dell'Università and Sezione INFN, Catania, Italy
²⁸Dipartimento di Fisica e Astronomia dell'Università and Sezione INFN, Padova, Italy
²⁹Dipartimento di Fisica e Nucleare e Teorica, Università di Pavia and Sezione INFN, Pavia, Italy
³⁰Dipartimento di Fisica 'E.R. Caianiello' dell'Università and Gruppo Collegato INFN, Salerno, Italy

- ³¹*Dipartimento DISAT del Politecnico and Sezione INFN, Turin, Italy*
- ³²*Dipartimento di Scienze e Innovazione Tecnologica dell'Università del Piemonte Orientale and INFN Sezione di Torino, Alessandria, Italy*
- ³³*Dipartimento di Scienze MIFT, Università di Messina, Messina, Italy*
- ³⁴*Dipartimento Interateneo di Fisica 'M. Merlin' and Sezione INFN, Bari, Italy*
- ³⁵*European Organization for Nuclear Research (CERN), Geneva, Switzerland*
- ³⁶*Faculty of Electrical Engineering, Mechanical Engineering and Naval Architecture, University of Split, Split, Croatia*
- ³⁷*Faculty of Engineering and Science, Western Norway University of Applied Sciences, Bergen, Norway*
- ³⁸*Faculty of Nuclear Sciences and Physical Engineering, Czech Technical University in Prague, Prague, Czech Republic*
- ³⁹*Faculty of Science, P.J. Šafárik University, Košice, Slovakia*
- ⁴⁰*Frankfurt Institute for Advanced Studies, Johann Wolfgang Goethe-Universität Frankfurt, Frankfurt, Germany*
- ⁴¹*Fudan University, Shanghai, China*
- ⁴²*Gangneung-Wonju National University, Gangneung, Republic of Korea*
- ⁴³*Gauhati University, Department of Physics, Guwahati, India*
- ⁴⁴*Helmholtz-Institut für Strahlen- und Kernphysik, Rheinische Friedrich-Wilhelms-Universität Bonn, Bonn, Germany*
- ⁴⁵*Helsinki Institute of Physics (HIP), Helsinki, Finland*
- ⁴⁶*High Energy Physics Group, Universidad Autónoma de Puebla, Puebla, Mexico*
- ⁴⁷*Hiroshima University, Hiroshima, Japan*
- ⁴⁸*Hochschule Worms, Zentrum für Technologietransfer und Telekommunikation (ZTT), Worms, Germany*
- ⁴⁹*Horia Hulubei National Institute of Physics and Nuclear Engineering, Bucharest, Romania*
- ⁵⁰*Indian Institute of Technology Bombay (IIT), Mumbai, India*
- ⁵¹*Indian Institute of Technology Indore, Indore, India*
- ⁵²*Indonesian Institute of Sciences, Jakarta, Indonesia*
- ⁵³*INFN, Laboratori Nazionali di Frascati, Frascati, Italy*
- ⁵⁴*INFN, Sezione di Bari, Bari, Italy*
- ⁵⁵*INFN, Sezione di Bologna, Bologna, Italy*
- ⁵⁶*INFN, Sezione di Cagliari, Cagliari, Italy*
- ⁵⁷*INFN, Sezione di Catania, Catania, Italy*
- ⁵⁸*INFN, Sezione di Padova, Padova, Italy*
- ⁵⁹*INFN, Sezione di Roma, Rome, Italy*
- ⁶⁰*INFN, Sezione di Torino, Turin, Italy*
- ⁶¹*INFN, Sezione di Trieste, Trieste, Italy*
- ⁶²*Inha University, Incheon, Republic of Korea*
- ⁶³*Institute for Gravitational and Subatomic Physics (GRASP), Utrecht University/Nikhef, Utrecht, Netherlands*
- ⁶⁴*Institute for Nuclear Research, Academy of Sciences, Moscow, Russia*
- ⁶⁵*Institute of Experimental Physics, Slovak Academy of Sciences, Košice, Slovakia*
- ⁶⁶*Institute of Physics, Homi Bhabha National Institute, Bhubaneswar, India*
- ⁶⁷*Institute of Physics of the Czech Academy of Sciences, Prague, Czech Republic*
- ⁶⁸*Institute of Space Science (ISS), Bucharest, Romania*
- ⁶⁹*Institut für Kernphysik, Johann Wolfgang Goethe-Universität Frankfurt, Frankfurt, Germany*
- ⁷⁰*Instituto de Ciencias Nucleares, Universidad Nacional Autónoma de México, Mexico City, Mexico*
- ⁷¹*Instituto de Física, Universidade Federal do Rio Grande do Sul (UFRGS), Porto Alegre, Brazil*
- ⁷²*Instituto de Física, Universidad Nacional Autónoma de México, Mexico City, Mexico*
- ⁷³*iThemba LABS, National Research Foundation, Somerset West, South Africa*
- ⁷⁴*Jeonbuk National University, Jeonju, Republic of Korea*
- ⁷⁵*Johann-Wolfgang-Goethe Universität Frankfurt Institut für Informatik, Fachbereich Informatik und Mathematik, Frankfurt, Germany*
- ⁷⁶*Joint Institute for Nuclear Research (JINR), Dubna, Russia*
- ⁷⁷*Korea Institute of Science and Technology Information, Daejeon, Republic of Korea*
- ⁷⁸*KTO Karatay University, Konya, Turkey*
- ⁷⁹*Laboratoire de Physique des 2 Infinis, Irène Joliot-Curie, Orsay, France*
- ⁸⁰*Laboratoire de Physique Subatomique et de Cosmologie, Université Grenoble-Alpes, CNRS-IN2P3, Grenoble, France*
- ⁸¹*Lawrence Berkeley National Laboratory, Berkeley, California, USA*
- ⁸²*Lund University Department of Physics, Division of Particle Physics, Lund, Sweden*
- ⁸³*Moscow Institute for Physics and Technology, Moscow, Russia*
- ⁸⁴*Nagasaki Institute of Applied Science, Nagasaki, Japan*
- ⁸⁵*Nara Women's University (NWU), Nara, Japan*
- ⁸⁶*National and Kapodistrian University of Athens, School of Science, Department of Physics, Athens, Greece*
- ⁸⁷*National Centre for Nuclear Research, Warsaw, Poland*

- ⁸⁸*National Institute of Science Education and Research, Homi Bhabha National Institute, Jatni, India*
- ⁸⁹*National Nuclear Research Center, Baku, Azerbaijan*
- ⁹⁰*National Research Centre Kurchatov Institute, Moscow, Russia*
- ⁹¹*Niels Bohr Institute, University of Copenhagen, Copenhagen, Denmark*
- ⁹²*Nikhef, National institute for subatomic physics, Amsterdam, Netherlands*
- ⁹³*NRC Kurchatov Institute IHEP, Protvino, Russia*
- ⁹⁴*NRC «Kurchatov»Institute - ITEP, Moscow, Russia*
- ⁹⁵*NRNU Moscow Engineering Physics Institute, Moscow, Russia*
- ⁹⁶*Nuclear Physics Group, STFC Daresbury Laboratory, Daresbury, United Kingdom*
- ⁹⁷*Nuclear Physics Institute of the Czech Academy of Sciences, Řež u Prahy, Czech Republic*
- ⁹⁸*Oak Ridge National Laboratory, Oak Ridge, Tennessee, USA*
- ⁹⁹*Ohio State University, Columbus, Ohio, USA*
- ¹⁰⁰*Petersburg Nuclear Physics Institute, Gatchina, Russia*
- ¹⁰¹*Physics department, Faculty of science, University of Zagreb, Zagreb, Croatia*
- ¹⁰²*Physics Department, Panjab University, Chandigarh, India*
- ¹⁰³*Physics Department, University of Jammu, Jammu, India*
- ¹⁰⁴*Physics Department, University of Rajasthan, Jaipur, India*
- ¹⁰⁵*Physikalisches Institut, Eberhard-Karls-Universität Tübingen, Tübingen, Germany*
- ¹⁰⁶*Physikalisches Institut, Ruprecht-Karls-Universität Heidelberg, Heidelberg, Germany*
- ¹⁰⁷*Physik Department, Technische Universität München, Munich, Germany*
- ¹⁰⁸*Politecnico di Bari and Sezione INFN, Bari, Italy*
- ¹⁰⁹*Research Division and ExtreMe Matter Institute EMMI, GSI Helmholtzzentrum für Schwerionenforschung GmbH, Darmstadt, Germany*
- ¹¹⁰*Rudjer Bošković Institute, Zagreb, Croatia*
- ¹¹¹*Russian Federal Nuclear Center (VNIIEF), Sarov, Russia*
- ¹¹²*Saha Institute of Nuclear Physics, Homi Bhabha National Institute, Kolkata, India*
- ¹¹³*School of Physics and Astronomy, University of Birmingham, Birmingham, United Kingdom*
- ¹¹⁴*Sección Física, Departamento de Ciencias, Pontificia Universidad Católica del Perú, Lima, Peru*
- ¹¹⁵*St. Petersburg State University, St. Petersburg, Russia*
- ¹¹⁶*Stefan Meyer Institut für Subatomare Physik (SMI), Vienna, Austria*
- ¹¹⁷*SUBATECH, IMT Atlantique, Université de Nantes, CNRS-IN2P3, Nantes, France*
- ¹¹⁸*Suranaree University of Technology, Nakhon Ratchasima, Thailand*
- ¹¹⁹*Technical University of Košice, Košice, Slovakia*
- ¹²⁰*The Henryk Niewodniczanski Institute of Nuclear Physics, Polish Academy of Sciences, Cracow, Poland*
- ¹²¹*The University of Texas at Austin, Austin, Texas, USA*
- ¹²²*Universidad Autónoma de Sinaloa, Culiacán, Mexico*
- ¹²³*Universidade de São Paulo (USP), São Paulo, Brazil*
- ¹²⁴*Universidade Estadual de Campinas (UNICAMP), Campinas, Brazil*
- ¹²⁵*Universidade Federal do ABC, Santo Andre, Brazil*
- ¹²⁶*University of Cape Town, Cape Town, South Africa*
- ¹²⁷*University of Houston, Houston, Texas, USA*
- ¹²⁸*University of Jyväskylä, Jyväskylä, Finland*
- ¹²⁹*University of Liverpool, Liverpool, United Kingdom*
- ¹³⁰*University of Science and Technology of China, Hefei, China*
- ¹³¹*University of South-Eastern Norway, Tonsberg, Norway*
- ¹³²*University of Tennessee, Knoxville, Tennessee, USA*
- ¹³³*University of the Witwatersrand, Johannesburg, South Africa*
- ¹³⁴*University of Tokyo, Tokyo, Japan*
- ¹³⁵*University of Tsukuba, Tsukuba, Japan*
- ¹³⁶*Université Clermont Auvergne, CNRS/IN2P3, LPC, Clermont-Ferrand, France*
- ¹³⁷*Université de Lyon, CNRS/IN2P3, Institut de Physique des 2 Infinis de Lyon, Lyon, France*
- ¹³⁸*Université de Strasbourg, CNRS, IPHC UMR 7178, F-67000 Strasbourg, France, Strasbourg, France*
- ¹³⁹*Université Paris-Saclay Centre d'Etudes de Saclay (CEA), IRFU, Département de Physique Nucléaire (DPHn), Saclay, France*
- ¹⁴⁰*Università degli Studi di Foggia, Foggia, Italy*
- ¹⁴¹*Università di Brescia and Sezione INFN, Brescia, Italy*
- ¹⁴²*Variable Energy Cyclotron Centre, Homi Bhabha National Institute, Kolkata, India*
- ¹⁴³*Warsaw University of Technology, Warsaw, Poland*
- ¹⁴⁴*Wayne State University, Detroit, Michigan, USA*
- ¹⁴⁵*Westfälische Wilhelms-Universität Münster, Institut für Kernphysik, Münster, Germany*
- ¹⁴⁶*Wigner Research Centre for Physics, Budapest, Hungary*

¹⁴⁷*Yale University, New Haven, Connecticut, USA*

¹⁴⁸*Yonsei University, Seoul, Republic of Korea*

^aAlso at Italian National Agency for New Technologies, Energy, Sustainable Economic Development (ENEA), Bologna, Italy.

^bAlso at Dipartimento DET del Politecnico di Torino, Turin, Italy.

^cDeceased.

^dAlso at M.V. Lomonosov Moscow State University, D.V. Skobeltsyn Institute of Nuclear, Physics, Moscow, Russia.

^eAlso at Institute of Theoretical Physics, University of Wrocław, Poland.